2010

Path Following for Unmanned Aerial Vehicles Using L1 Adaptive Augmentation of Commercial Autopilots

Kaminer, Isaac

JOURNAL OF GUIDANCE, CONTROL, AND DYNAMICS
Vol. 33, No. 2, March–April 2010

Path Following for Unmanned Aerial Vehicles Using $\mathcal{L}_1$ Adaptive Augmentation of Commercial Autopilots

Isaac Kaminer*
Naval Postgraduate School, Monterey, California 93943
António Pascoal†
Instituto Superior Técnico, Lisbon, 1049 Portugal
Enric Xargay‡ and Naira Hovakimyan§
University of Illinois at Urbana–Champaign, Urbana, Illinois 61801
Chengyu Cao¶
University of Connecticut, Storrs, Connecticut 06269
and
Vladimir Dobrokhodov**
Naval Postgraduate School, Monterey, California 93943

DOI: 10.2514/1.42056

The paper presents a three-dimensional path-following control algorithm that expands the capabilities of conventional autopilots, which are normally designed to provide only guidance loops for waypoint navigation. Implementation of this algorithm broadens the range of possible applications of small unmanned aerial vehicles. The solution proposed takes explicit advantage of the fact that normally these vehicles are equipped with autopilots stabilizing the vehicles and providing angular-rate tracking capabilities. Therefore, the overall closed-loop system exhibits naturally an inner–outer (dynamics–kinematics) control loop structure. The outer-loop path-following control law developed relies on a nonlinear control strategy derived at the kinematic level, while the inner-loop consisting of the autopilot together with an $\mathcal{L}_1$ adaptive augmentation loop is designed to meet strict performance requirements in the presence of unmanned aerial vehicle modeling uncertainty and environmental disturbances. A rigorous proof of stability and performance of the path-following closed-loop system, including the dynamics of the unmanned aerial vehicle with its autopilot, is given. The paper bridges the gap between theory and practice and includes results of extensive flight tests performed in Camp Roberts, California, which demonstrate the benefits of the framework adopted for the control system design.

I. Introduction

UNMANNED aerial vehicles (UAVs) play an increasingly important role in a large number of civilian and military missions. Examples include military reconnaissance and strike operations, border patrol missions, forest fire detection, police surveillance, and recovery operations. For most of these operations, it is critical that the UAVs involved be capable of following spatial paths with good accuracy. In this paper we define path following as the ability to follow a 3-D path for any feasible speed profile††. Motivated by this requirement, this paper proposes a solution to the problem of UAV path following that yields an inner–outer (dynamics–kinematics) control structure, thus taking advantage of the autopilots (APs) that are normally installed on board UAVs. To this effect, a theoretical framework is developed to augment the existing autopilot of a UAV that is tasked to follow a specified path defined by the particular mission at hand. The adaptive augmentation loop effectively ensures that the autopilot can track the commands issued by a properly designed outer-loop path-following algorithm. Since autopilots are normally designed to provide only waypoint navigation, the proposed framework significantly expands the span of their applications by providing UAVs with path-following capabilities.

Pioneering work in the area of path following can be found in [1], where an elegant solution to the problem was presented for a wheeled robot at the kinematic level. In the setup adopted, the kinematic model of the vehicle was derived with respect to a Frenet–Serret frame moving along the path, playing the role of a virtual target vehicle to be tracked by the real vehicle. The origin of the Frenet–Serret was placed at the point on the path closest to the real vehicle.

The initial work in [1] has spurred a great deal of activity in the literature addressing the path-following problem. A popular approach that emerged was to solve a trajectory tracking problem and then reparameterize the resulting feedback controller using an independent variable other than time. See, for example, [2–4], and references therein. Furthermore, the approach of [1] was extended to UAVs in [5], where the authors addressed the issue of path following of trimming trajectories and derived nonlinear path-following controllers that satisfy a so-called linearization property and to autonomous underwater vehicles (AUVs) in [6], where a backstepping approach was used to determine a nonlinear path-following controller. The common feature of the latter papers was to reduce the path-following problem to that of driving the kinematic errors

Received 6 November 2008; revision received 15 November 2009; accepted for publication 16 November 2009.

*Professor, Department of Mechanical and Astronautical Engineering; kaminer@nps.edu. Member AIAA.
†Associate Professor, Department of Electrical Engineering and Institute for Systems and Robotics; antonio@isr.ist.utl.pt. Member AIAA
‡Doctoral Student, Department of Aerospace Engineering; xargay@illinois.edu. Student Member AIAA.
§Professor, Department of Mechanical Science and Engineering; nhovakim@illinois.edu. Associate Fellow AIAA.
¶Assistant Professor, Department of Mechanical Engineering; ccao@engr.uconn.edu. Member AIAA.
**Assistant Professor, Department of Mechanical and Astronautical Engineering; vldobr@nps.edu. Senior Member AIAA.

††This is opposite to trajectory tracking that requires a vehicle to track a 4-D path, i.e., to be at a given point in space at a prespecified time.

resolved in Frenet–Serret frame to zero. This approach ensures that path following is essentially done by proper choice of the vehicle's attitude, a strategy that is akin to that used by pilots when they fly airplanes. The same cannot be said of the work reported in [2–4].

The setup used in [1] was later reformulated in [7], leading to a feedback control law that steers the dynamic model of a wheeled robot along a desired path and overcomes some of the constraints present in [1]. The key to this new algorithm was to add another degree of freedom to the rate of progression of the virtual target, in contrast with the strategy for placement of the origin of the Frenet–Serret frame adopted in [1]. In the present paper, the algorithm presented in [7] is extended to the 3-D case for the control of a UAV at a kinematic level, and an adaptive augmentation loop based on $\mathcal{L}_1$ adaptive control theory [8,9] is introduced to deal with the UAV dynamics and meet strict performance requirements in the presence of plant uncertainty and external disturbances. The solution proposed for path following departs from standard backstepping techniques in that the final path-following control law makes explicit use of the existing UAV autopilot, resulting in a multiloop control structure that retains the properties of the autopilot, which is designed to stabilize the UAV. Namely, path-following control design is first done at a kinematic level, leading to an outer-loop controller that generates pitch and yaw rate commands to an inner-loop controller. The latter relies on an off-the-shelf autopilot for angular-rate command tracking, augmented with an $\mathcal{L}_1$ adaptive output feedback control law that guarantees stability and performance of the complete system. The main benefit of the $\mathcal{L}_1$ adaptive controller is its ability to yield fast and robust adaptation, as proven in [8,10]. Moreover, it has analytically computable performance bounds for the system's input and output signals simultaneously, in addition to its guaranteed time-delay margin [9]. The $\mathcal{L}_1$ adaptive controller has been used to augment existing controllers in several aircraft applications and has been found to exhibit excellent system performance. Moreover, unlike conventional adaptive control architectures, the $\mathcal{L}_1$ adaptive control methodology provides a systematic framework for the design of nonlinear adaptive control laws, which has the potential of reducing flight control design costs (see [11–19], for example).

The reader will find in [20,21] an extension of the framework developed in this paper, which tackles the problem of cooperative control of multiple UAVs executing time-critical missions. See also [22] for preliminary work on autopilot augmentation.

The paper is organized as follows. Section II formulates the path-following problem and describes the kinematics and dynamics of the systems of interest. In Sec. III, the path-following problem is solved at the kinematic level (outer-loop control). Section IV describes an $\mathcal{L}_1$ adaptive augmentation technique for path following that yields an inner-loop control structure and exploits the availability of off-the-shelf autopilots for pitch and yaw rate reference tracking. Section V presents actual flight test results performed in Camp Roberts, CA. Finally, Sec. VI summarizes the key results and contains the main conclusions.

Throughout the paper, $y(s)$ denotes the Laplace transform of the time signal $y(t)$. Also, unless otherwise mentioned, $\|\cdot\|$ will be used to denote the 2-norm of a vector.

II. Problem Formulation

This section formulates the problem of path-following control for a (single) UAV in 3-D space. We recall that path following refers to the problem of making a vehicle converge to and follow a desired feasible path described by some convenient parameter (e.g., path length). Although in general no time schedule is assigned to the path, one may assign a desired speed profile for the vehicle to track. The speed may itself be a function of the path parameter, time, or a combination thereof. We notice that this approach is in contrast to trajectory tracking, for which it has been proven in [23] that, in the presence of unstable zero dynamics, there are fundamental performance limitations that cannot be overcome by any controller structure.

For the missions of interest, we assume that

Assumption 1: Both the given path and the desired speed profile of the vehicle along the path satisfy boundary as well as appropriate feasibility conditions, such as those imposed by the physical limitations of the UAV. It is further assumed that the rate commands required to follow the path do not result in the UAV operating outside its normal flight envelope and do not lead to internal saturation of the AP.

The path-following algorithm proposed in this paper relies on the insight that a UAV can follow a given path using only its attitude while maintaining a given speed profile. Thus, the key idea of the proposed algorithm is to add a virtual target running along the path and to use the vehicle's attitude control effectors to follow this virtual target. It is therefore natural to introduce a frame attached to this virtual target and define a generalized error vector between this moving coordinate system and a frame attached to the UAV. With this setup, the path-following control problem can be reduced to driving this generalized error vector to zero by using vehicle attitude control effectors only. Then, as will become clear, the overall path-following system (including the aircraft dynamics as well as the AP) can be described by a cascade of two systems: 1) a system $\mathcal{G}_p$ describing the dynamics of the closed loop with the UAV and its AP; and 2) the dynamics $\mathcal{G}_e$ of the kinematic errors between the UAV and the virtual target running along the path. Figure 1 shows the resulting cascaded system. In what follows, we characterize the subsystems $\mathcal{G}_e$ and $\mathcal{G}_p$ separately.

A. Path-Following Kinematic-Error Equations

In this section we introduce the error dynamics defined at a kinematic level between a frame attached to the UAV and the frame attached to the virtual target running along the path. Figure 2 captures the geometry of the problem at hand. Let $\mathcal{I}$ denote an inertial frame, and let Q be the UAV center of mass. Further, let $p_c(\ell)$ be the path to be followed, parameterized by its path length ℓ, and P be an arbitrary point on the path that plays the role of the center of mass of the virtual target to be followed. Note that this is a different approach as compared with the setup for path following originally proposed in [1], where P was simply defined as the point on the path that is closest to the vehicle. Endowing P with an extra degree of freedom is the key to the algorithm presented in [7], which is extended in this paper to the 3-D case.

Let $\mathcal{F}$ be a parallel transport frame [24,25] attached to the point P on the path, and let $T(\ell)$, $N_1(\ell)$ and $N_2(\ell)$ be orthonormal vectors satisfying the frame equations:

$$\begin{bmatrix} \frac{\mathrm{d}T(\ell)}{\mathrm{d}\ell} \\ \frac{\mathrm{d}N_1(\ell)}{\mathrm{d}\ell} \\ \frac{\mathrm{d}N_2(\ell)}{\mathrm{d}\ell} \end{bmatrix} = \begin{bmatrix} 0 & k_1(\ell) & k_2(\ell) \\ -k_1(\ell) & 0 & 0 \\ -k_2(\ell) & 0 & 0 \end{bmatrix} \begin{bmatrix} T(\ell) \\ N_1(\ell) \\ N_2(\ell) \end{bmatrix}$$

where the parameters $k_1(\ell)$ and $k_2(\ell)$ are related to the polar coordinates of curvature $\kappa(\ell)$ and torsion $\tau(\ell)$ as

$$\kappa(\ell) = (k_1^2(\ell) + k_2^2(\ell))^{\frac{1}{2}} \qquad \tau(\ell) = -\frac{\mathrm{d}}{\mathrm{d}\ell}\left(\tan^{-1}\left(\frac{k_2(\ell)}{k_1(\ell)}\right)\right)$$

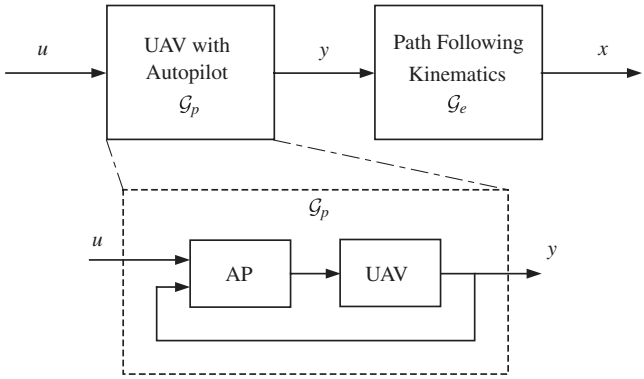

Fig. 1 Cascaded path-following error dynamics with closed-loop UAV with AP dynamics.

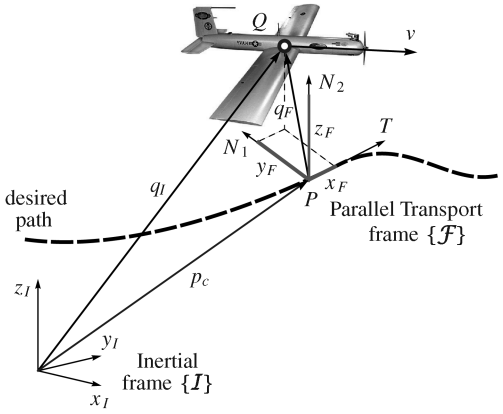

Fig. 2 Problem geometry.

We note that, unlike the Frenet–Serret frame, this moving frame is well-defined when the path has a vanishing second derivative. The vectors $T(\ell)$, $N_1(\ell)$ and $N_2(\ell)$ define an orthonormal basis for $\mathcal{F}$. Note that the unit vector $T(\ell)$ defines the tangent direction to the path at the point determined by ℓ, while $N_1(\ell)$ and $N_2(\ell)$ define the normal plane perpendicular to $T(\ell)$, and they can be used to construct the rotation matrix $R_F^I(\ell) = [\,T(\ell), \quad N_1(\ell), \quad N_2(\ell)\,]$ from $\mathcal{F}$ to $\mathcal{I}$. Denote by ω_{FI}^F the angular velocity of $\mathcal{F}$ with respect to $\mathcal{I}$, resolved in $\mathcal{F}$, which is given by

$$\omega_{FI}^F(t) = [\,0, \quad -k_2(\ell)\dot{\ell}(t), \quad k_1(\ell)\dot{\ell}(t)\,]^\top \tag{1}$$

Also, let

$$p_I(t) = [\,x_I(t), \quad y_I(t), \quad z_I(t)\,]^\top \tag{2}$$

be the position of the UAV center of mass Q resolved in $\mathcal{I}$, and let

$$p_F(t) = [\,x_F(t), \quad y_F(t), \quad z_F(t)\,]^\top \tag{3}$$

be the difference between $p_I(t)$ and $p_c(t)$ resolved in $\mathcal{F}$. Finally, let $\mathcal{W}'$ denote a coordinate system defined by projecting the wind frame $\mathcal{W}$ onto a local level plane. (The frame $\mathcal{W}'$ has its origin at Q and its x-axis is aligned with the UAV's velocity vector.)

Finally, let

$$\Phi_e(t) = [\,\phi_e(t), \quad \theta_e(t), \quad \psi_e(t)\,]^\top \tag{4}$$

denote the set of Euler angles that locally parameterize the rotation matrix from $\mathcal{F}$ to $\mathcal{W}'$. In what follows, $v(t)$ is the magnitude of the UAV's velocity vector, $\gamma(t)$ is the flight path angle, $\psi(t)$ is the ground heading angle, and $q(t)$ and $r(t)$ are the y-axis and z-axis components, respectively, of the vehicle's rotational velocity resolved in $\mathcal{W}'$ frame. For the purpose of this paper and with a slight abuse of notation, $q(t)$ and $r(t)$ will be referred to as pitch rate and yaw rate, respectively, in the $\mathcal{W}'$ frame.

With the above notation, the UAV kinematic equations can be written as

$$\begin{cases} \dot{x}_I = v\cos\gamma\cos\psi \\ \dot{y}_I = -v\cos\gamma\sin\psi \\ \dot{z}_I = v\sin\gamma \\ \dot{\gamma} = q \\ \dot{\psi} = \cos^{-1}\gamma r \end{cases} \tag{5}$$

Remark 1: Clearly, the UAV kinematic equations take a very simple form if we use the $\mathcal{W}'$ frame [see (5)]. In the next section we will take advantage of this simplicity to derive relatively straightforward path-following control laws.

From

$$p_I = p_c(\ell) + R_F^I p_F$$

it follows that

$$\dot{p}_I = R_F^I \begin{bmatrix} \dot{\ell} \\ 0 \\ 0 \end{bmatrix} + R_F^I \begin{bmatrix} \dot{x}_F \\ \dot{y}_F \\ \dot{z}_F \end{bmatrix} + R_F^I \left(\omega_{FI}^F \times \begin{bmatrix} x_F \\ y_F \\ z_F \end{bmatrix} \right) \tag{6}$$

Using (6) and the fact that

$$R_I^F \begin{bmatrix} \dot{x}_I \\ \dot{y}_I \\ \dot{z}_I \end{bmatrix} = R_{W'}^F R_I^{W'} \begin{bmatrix} \dot{x}_I \\ \dot{y}_I \\ \dot{z}_I \end{bmatrix} = R_{W'}^F \begin{bmatrix} v \\ 0 \\ 0 \end{bmatrix}$$

where $R_{W'}^F$ and $R_I^{W'}$ are the rotation matrices from $\mathcal{W}'$ to $\mathcal{F}$ and $\mathcal{I}$ to $\mathcal{W}'$, respectively, we obtain

$$R_I^F \begin{bmatrix} \dot{x}_I \\ \dot{y}_I \\ \dot{z}_I \end{bmatrix} = \begin{bmatrix} \dot{x}_F + \dot{\ell}(1 - k_1(\ell)y_F - k_2(\ell)z_F) \\ \dot{y}_F + \dot{\ell}k_1(\ell)x_F \\ \dot{z}_F + \dot{\ell}k_2(\ell)x_F \end{bmatrix}$$

which yields

$$\begin{bmatrix} \dot{x}_F \\ \dot{y}_F \\ \dot{z}_F \end{bmatrix} = \begin{bmatrix} -\dot{\ell}(1 - k_1(\ell)y_F - k_2(\ell)z_F) \\ -\dot{\ell}k_1(\ell)x_F \\ -\dot{\ell}k_2(\ell)x_F \end{bmatrix} + R_{W'}^F \begin{bmatrix} v \\ 0 \\ 0 \end{bmatrix} \tag{7}$$

Equation (7) describes the path-following kinematic position-error dynamics of the UAV with respect to the virtual target on the path.

Consider now the Euler kinematic equation

$$\dot{\Phi}_e = Q_\Phi^{-1}(\Phi_e)\omega_{W'F}^{W'} \tag{8}$$

where

$$Q_\Phi^{-1}(\Phi_e) = \begin{bmatrix} 1 & \sin\phi_e\tan\theta_e & \cos\phi_e\tan\theta_e \\ 0 & \cos\phi_e & -\sin\phi_e \\ 0 & \frac{\sin\phi_e}{\cos\theta_e} & \frac{\cos\phi_e}{\cos\theta_e} \end{bmatrix}$$

is nonsingular for $\theta_e \neq \pm\frac{\pi}{2}$ and $\omega_{W'F}^{W'}$ denotes the angular velocity of $\mathcal{W}'$ with respect to $\mathcal{F}$, resolved in $\mathcal{W}'$, given by

$$\omega_{W'F}^{W'} = \omega_{W'I}^{W'} - \omega_{FI}^{W'}$$

where $\omega_{FI}^{W'} = R_F^{W'}\omega_{FI}^F$. Equation (8) can be rewritten as

$$\dot{\Phi}_e = Q_\Phi^{-1}(\Phi_e)(\omega_{W'I}^{W'} - R_F^{W'}\omega_{FI}^F) \tag{9}$$

which yields

$$\begin{bmatrix} \dot{\theta}_e \\ \dot{\psi}_e \end{bmatrix} = \underbrace{\begin{bmatrix} \dot{\ell}k_2(\ell)\cos\psi_e \\ -\dot{\ell}(k_1(\ell) - k_2(\ell)\tan\theta_e\sin\psi_e) \end{bmatrix}}_{\triangleq D(t,\theta_e,\psi_e)} + \underbrace{\begin{bmatrix} \cos\phi_e & -\sin\phi_e \\ \frac{\sin\phi_e}{\cos\theta_e} & \frac{\cos\phi_e}{\cos\theta_e} \end{bmatrix}}_{\triangleq T(t,\theta_e)} \begin{bmatrix} q \\ r \end{bmatrix} \tag{10}$$

where both $D(t,\theta_e,\psi_e)$ and $T(t,\theta_e)$ are well-defined for all $\theta_e \neq \pm\frac{\pi}{2}$. Equation (10) describes the path-following kinematic attitude-error dynamics of the frame attached to the UAV with respect to the frame attached to the virtual target. Combining Eqs. (7) and (10) gives the path-following kinematic-error dynamics

$$\mathcal{G}_e: \begin{cases} \dot{x}_F = -\dot{\ell}(1 - k_1(\ell)y_F - k_2(\ell)z_F) + v\cos\theta_e\cos\psi_e \\ \dot{y}_F = -\dot{\ell}k_1(\ell)x_F + v\cos\theta_e\sin\psi_e \\ \dot{z}_F = -\dot{\ell}k_2(\ell)x_F - v\sin\theta_e \\ \dot{\theta}_e = \dot{\ell}k_2(\ell)\cos\psi_e + \cos\phi_e q - \sin\phi_e r \\ \dot{\psi}_e = -\dot{\ell}(k_1(\ell) - k_2(\ell)\tan\theta_e\sin\psi_e) + \frac{\sin\phi_e}{\cos\theta_e}q + \frac{\cos\phi_e}{\cos\theta_e}r \end{cases} \tag{11}$$

Note that in the kinematic-error model (11), $q(t)$ and $r(t)$ play the role of virtual control inputs. Notice also how the rate of progression

$\dot{\ell}(t)$ of the point P along the path becomes an extra variable that can be manipulated at will.

At this point, it is convenient to formally define the state vector for the path-following kinematic-error dynamics as

$$x(t) = [\, x_F(t), \quad y_F(t), \quad z_F(t), \quad \theta_e(t) - \delta_\theta(t), \quad \psi_e(t) - \delta_\psi(t)\,]^\top$$

where

$$\delta_\theta(t) = \sin^{-1}\left(\frac{z_F(t)}{|z_F(t)| + d_1}\right), \quad \delta_\psi(t) = \sin^{-1}\left(\frac{-y_F(t)}{|y_F(t)| + d_2}\right) \tag{12}$$

with d_1 and d_2 being some positive constants. Notice that, instead of the angular errors $\theta_e(t)$ and $\psi_e(t)$, we use $\theta_e(t) - \delta_\theta(t)$ and $\psi_e(t) - \delta_\psi(t)$, respectively, to shape the approach angles to the path. Clearly, when the vehicle is far from the desired path the approach angles become close to $\pi/2$. As the vehicle comes closer to the path, the approach angles tend to zero. The system $\mathcal{G}_e$ is now completely characterized by defining the vector of input signals as

$$y(t) = [\, q(t), \quad r(t)\,]^\top$$

B. Unmanned Aerial Vehicle with Autopilot

At this level, only the kinematic equations of the UAV have been considered, for which the pitch rate $q(t)$ and the yaw rate $r(t)$ are the control inputs. Next, we consider the closed-loop dynamics of the UAV with the AP (subsystem $\mathcal{G}_p$).

Assumption 2: It is assumed that the AP was designed to stabilize the UAV and to provide angular rate as well as airspeed tracking capabilities.

First, we note that Assumption 1 implies that the speed profile will be bounded above and below. Second, from this fact and from Assumption 2, one can conclude that the UAV airspeed satisfies:

$$0 < v_{\min} \le v(t) \le v_{\max}, \quad \forall\ t \ge 0 \tag{13}$$

Moreover, for the purpose of this paper, we will consider only the pitch rate and yaw rate closed-loop dynamics and thus the subsystem $\mathcal{G}_p$ will define only the dynamics from the angular rate commands $u(t) = [q_{\text{ad}}(t), r_{\text{ad}}(t)]^\top$, to the respective actual UAV angular rates $y(t) = [q(t), r(t)]^\top$. We note that other dynamics, like roll dynamics, need not be included in this model since the key idea behind the path-following algorithm is to take explicit advantage of the onboard AP and use pitch rate and yaw rate commands to make the vehicle follow the path. In this sense, it is the AP that determines the bank angle required to track the angular-rate commands. Therefore, it is justified to assume that

Assumption 3: The UAV roll dynamics (roll rate and bank angle) will be bounded for bounded angular-rate commands corresponding to the set of feasible paths considered.

We also observe that typical off-the-shelf APs are capable of providing uniform performance across the flight envelope of small UAVs and, for the missions of interest, which are limited to small bank angles, can be designed to achieve satisfactory decoupling between the longitudinal and lateral/directional channels[‡‡]. We, therefore, make the reasonable assumption in this paper that the dynamics of the closed-loop system consisting of the UAV and its AP assume the (decoupled) form

$$\mathcal{G}_p: \begin{cases} q(s) = G_q(s)(q_{ad}(s) + z_q(s)) \\ r(s) = G_r(s)(r_{ad}(s) + z_r(s)) \end{cases} \tag{14}$$

where $G_q(s)$, $G_r(s)$ are unknown strictly proper and stable transfer functions for which only lower bounds d_{G_q} and d_{G_r} on their relative degrees are known; $z_q(s)$, $z_r(s)$ represent the Laplace transforms of time-varying uncertainties and disturbance signals $z_q(t)$= $f_q(t, q(t))$ and $z_r(t) = f_r(t, r(t))$, respectively, while f_q and f_r are unknown nonlinear maps subject to the following assumptions:

Assumption 4: There exist positive constants L_q, L_{q0}, L_r, and L_{r0} such that the inequalities

$$|f_q(t, q_1) - f_q(t, q_2)| \le L_q|q_1 - q_2|, \quad |f_q(t, q)| \le L_q|q| + L_{q0}$$
$$|f_r(t, r_1) - f_r(t, r_2)| \le L_r|r_1 - r_2|, \quad |f_r(t, r)| \le L_r|r| + L_{r0}$$

hold uniformly in $t \ge 0$.

Assumption 5: There exist positive constants L_{q1}, L_{q2}, L_{q3}, L_{r1}, L_{r2}, and L_{r3} such that for all $t \ge 0$:

$$|\dot{z}_q(t)| \le L_{q1}|\dot{q}(t)| + L_{q2}|q(t)| + L_{q3}$$
$$|\dot{z}_r(t)| \le L_{r1}|\dot{r}(t)| + L_{r2}|r(t)| + L_{r3}$$

We note that only very limited knowledge of the feedback system consisting of the UAV and autopilot (inner loop) is assumed at this point. In fact, we do not require that the orders of the unknown transfer functions $G_q(s)$ and $G_r(s)$ be known. We only assume that these are strictly proper and stable, with a known lower bound on their relative degrees. We nevertheless notice that the bandwidth of the control channel of the closed-loop UAV with the autopilot is very limited, and the model (14) is valid only for the low-frequency approximation of $\mathcal{G}_p$.

In summary, the key subsystems in the overall path-following system (including the autopilot and the UAV dynamics) can be described by a cascaded structure of the form

$$\mathcal{G}_e: \dot{x}(t) = f(x(t)) + g(x(t))y(t) \tag{15}$$

$$\mathcal{G}_p: y(s) = G_p(s)(u(s) + z(s)) \tag{16}$$

where subsystem $\mathcal{G}_e$ represents the path-following kinematic-error dynamics between the UAV and the virtual target, and subsystem $\mathcal{G}_p$ models the closed-loop system of the UAV with its AP. The maps f and g are known, whereas $G_p(s)$ is an unknown strictly proper and stable transfer matrix. We note that $x(t)$ and $y(t)$ are the only measured outputs of this cascaded system and $u(t)$ is the only control input, while $z(t)$ models unknown time-varying uncertainties. Finally, $y(s)$, $u(s)$ and $z(s)$ denote the Laplace transformations of $y(t)$, $u(t)$ and $z(t)$, respectively.

Using the above formulation we now define the path-following problem (PFP) to be solved in this paper as:

Definition 1 (PFP): Using Assumptions 1 through 5 and given a desired path $p_c(\ell)$ to be followed, the control objective is to stabilize $x(t)$ in (15) by proper design of $u(t)$ in (16) without any modifications to the AP.

In what follows we propose a solution to this problem that includes two steps: 1) solving the PFP at the kinematic level; and 2) using the solution obtained in step 1 to derive a controller for the complete system.

III. Stabilizing Function for the Path-Following Kinematics

The dynamics of a typical autonomous vehicle are usually represented by a system of high order nonlinear differential equations that include vehicle dynamics and kinematics. Commercially, the problem of controlling such systems is tackled by 1) designing an inner-loop controller to stabilize the vehicle dynamics, and 2) designing an outer-loop controller to control vehicle kinematics. We propose to solve the path-following problem using the same inner/outer-loop structure. At the outer-loop level, vehicle kinematics are employed to solve the path-following problem using vehicle attitude rates as control inputs. At the inner-loop level, vehicle attitude rates are tracked by the off-the-shelf autopilot augmented by the $\mathcal{L}_1$ adaptive loop so as to guarantee overall system stability and performance specifications.

The derivation of the path-following control loop is done by following a constructive approach. In this section, only the simplified

[‡‡]This can be achieved by introducing coupling from bank angle to elevator inside the AP.

kinematic equations of the vehicle will be addressed by taking pitch rate and turn rate as virtual outer-loop control inputs. In particular, we show that, in the ideal case of a point-mass UAV (obtained by neglecting the closed-loop dynamics of the UAV with its AP), there exist stabilizing functions for $q(t)$ and $r(t)$ leading to local exponential stability of the origin of $\mathcal{G}_e$ with a prescribed domain of attraction. Figure 3 presents the kinematic closed-loop system considered. We note that the point-mass assumption will be dropped later in Sec. IV, and the closed-loop dynamics of the UAV with its AP will be included in the path-following problem.

We start by assuming that the UAV speed satisfies the bounds in (13). Also, given an arbitrary positive constant c, let c_1 and c_2 be positive constants that satisfy the inequality

$$v_i \triangleq \sqrt{cc_2} + \sin^{-1}\left(\frac{\sqrt{cc_1}}{\sqrt{cc_1}+d_i}\right) \leq \frac{\pi}{2} - \epsilon_i, \qquad i = 1,2 \tag{17}$$

where d_1 and d_2 were introduced in (12), and ϵ_1 and ϵ_2 are positive constants such that $0 < \epsilon_i < \frac{\pi}{2}$, $i = 1, 2$. Let the rate of progression of point P along the path be governed by

$$\dot{\ell}(t) = K_1 x_F(t) + v(t)\cos\theta_e(t)\cos\psi_e(t) \tag{18}$$

where $K_1 > 0$. Then, the input vector $y_c(t)$ given by

$$y_c(t) = \begin{bmatrix} q_c(t) \\ r_c(t) \end{bmatrix} = T^{-1}(t,\theta_e)\left(\begin{bmatrix} u_{\theta_c}(t) \\ u_{\psi_c}(t) \end{bmatrix} - D(t,\theta_e,\psi_e)\right) \tag{19}$$

where $T(t,\theta_e)$ and $D(t,\theta_e,\psi_e)$ were introduced in (10) and $u_{\theta_c}(t)$ and $u_{\psi_c}(t)$ are defined as

$$\begin{aligned} u_{\theta_c}(t) &= -K_2(\theta_e(t) - \delta_\theta(t)) \\ &\quad + \frac{c_2}{c_1} z_F(t) v(t) \frac{\sin\theta_e(t) - \sin\delta_\theta(t)}{\theta_e(t) - \delta_\theta(t)} + \dot{\delta}_\theta(t) \\ u_{\psi_c}(t) &= -K_3(\psi_e(t) - \delta_\psi(t)) \\ &\quad - \frac{c_2}{c_1} y_F(t) v(t)\cos\theta_e(t) \frac{\sin\psi_e(t) - \sin\delta_\psi(t)}{\psi_e(t) - \delta_\psi(t)} + \dot{\delta}_\psi(t) \end{aligned} \tag{20}$$

stabilizes the subsystem $\mathcal{G}_e$ for any $K_2 > 0$ and $K_3 > 0$. A formal statement of this key result is given in the lemma below.

Lemma 1: Let the progression of point P along the path be governed by (18). Then, for any $v(t)$ verifying (13), the origin of the kinematic-error equations in (11) with the controllers $q(t) \equiv q_c(t)$, $r(t) \equiv r_c(t)$ defined in (19) and (20) is exponentially stable with the domain of attraction

$$\Omega = \left\{ x:\ V_{\text{pf}}(x) < \frac{c}{2} \right\} \tag{21}$$

with

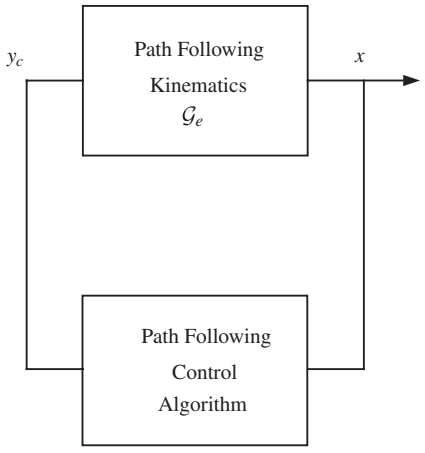

Fig. 3 Path-following closed-loop system solved at a kinematic level.

$$V_{\text{pf}}(x) = x^\top P_{\text{pf}} x, \quad P_{\text{pf}} = \text{diag}\left(\frac{1}{2c_1}, \frac{1}{2c_1}, \frac{1}{2c_1}, \frac{1}{2c_2}, \frac{1}{2c_2}\right) \tag{22}$$

where c, c_1, and c_2 were introduced in (17).

The proof is given in the Appendix. □

Remark 2: Notice that the solution to the path-following problem assumes only that $v(t)$ is bounded below but is otherwise undefined. The speed profile $v(t)$ can therefore be seen as an extra degree of freedom, which could be used, for example, to solve a problem of time-critical coordination involving multiple UAVs [20,21].

Remark 3: The control law (19) and (20) produces angular-rate commands defined in the $\mathcal{W}'$ frame. However, a typical commercial autopilot accepts rate commands defined in body-fixed frame $\mathcal{B}$. The coordinate transformation from $\mathcal{W}'$ to $\mathcal{B}$ is given by

$$R^{\mathcal{B}}_{\mathcal{W}'} = R^{\mathcal{B}}_{\mathcal{W}} R^{\mathcal{W}}_{\mathcal{W}'}$$

where the transformation $R^{\mathcal{B}}_{\mathcal{W}}$ is defined using the angle of attack and the sideslip angle. For the UAVs considered in this paper, these angles are usually small, and, therefore, it is reasonable to assume that $R^{\mathcal{B}}_{\mathcal{W}} \approx \mathbb{I}$. On the other hand, $R^{\mathcal{W}}_{\mathcal{W}'}$ is defined via a single rotation around a local x-axis by an angle ϕ_W. For small values of angle of attack and sideslip angle, ϕ_W can be approximated by the body-fixed bank-angle ϕ measured by a typical autopilot. Therefore, in the final implementation, the angular-rate commands (19) and (20) are resolved in the body-fixed frame $\mathcal{B}$ using the transformation discussed here.

Thus, in the following sections we assume that both the autopilot angular rates $y(t) = [q(t), \quad r(t)]^\top$ and the commanded angular rates $y_c(t) = [q_c(t), \quad r_c(t)]^\top$ are resolved in $\mathcal{W}'$. We notice that this assumption will not affect the results since,

$$\|(y(t) - y_c(t))^{\mathcal{W}'}\| = \|(y(t) - y_c(t))^{\mathcal{B}}\|$$

IV. Path Following with $\mathcal{L}_1$ Adaptive Augmentation

In the preceding section, we showed that for the point-mass case, the stabilizing control laws in (19) and (20) lead to local exponential stability of the origin of $\mathcal{G}_e$ with a prescribed domain of attraction. In this section, we remove the point-mass assumption and include the UAV dynamics in the path-following problem.

Clearly, to make the UAV follow a path with a prespecified level of accuracy, it is necessary to ensure that the UAV is capable of tracking with desired performance specifications the angular-rate commands generated by the outer-loop path-following controller in (19) and (20). Conventional gain-scheduled APs can be tuned to achieve satisfactory tracking capabilities. However, fine-tuning of such controllers can be time consuming and very expensive. In fact, the effort and cost in AP fine tuning can be reduced by wrapping an adaptive augmentation loop around the AP. Inner-loop adaptive flight control systems provide also the opportunity of improving aircraft performance across the flight envelope in the event of control surface failures, vehicle damage, and in the presence of environmental disturbances.

In this section, the autopilot is first augmented with an $\mathcal{L}_1$ adaptive output feedback controller to ensure that the closed-loop UAV with the autopilot tracks the commands $q_c(t)$ and $r_c(t)$ generated by the path-following algorithm in the presence of unmodeled dynamics and bounded disturbances. In particular, we derive computable uniform performance bounds for the adaptive closed-loop system with respect to the reference input signals. Then, these performance bounds of the $\mathcal{L}_1$ adaptive controller are used to prove stability of the path-following closed-loop system taking into account the dynamics of the UAV with its AP (see Fig. 4).

A. Definitions

To streamline the subsequent analysis, we need to recall some basic definitions and facts from linear system theory [26].

Definition 2: ($\mathcal{L}_\infty$-norm and truncated $\mathcal{L}_\infty$-norm) for a signal $\xi(t)$, $t \geq 0$, $\xi \in \mathbb{R}^n$, its truncated $\mathcal{L}_\infty$- and $\mathcal{L}_\infty$-norms are defined, respectively, as:

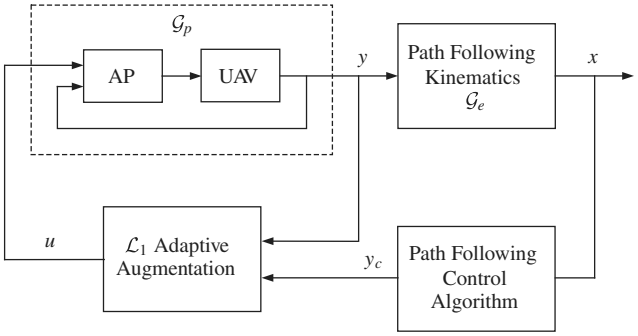

Fig. 4 Closed-loop cascaded system with $\mathcal{L}_1$ adaptive augmentation.

$$\|\xi_t\|_{\mathcal{L}_\infty} = \max_{i=1,\ldots,n} \left(\sup_{0\le\tau\le t} |\xi_i(\tau)| \right) \qquad \|\xi\|_{\mathcal{L}_\infty} = \max_{i=1,\ldots,n} \left(\sup_{\tau\ge 0} |\xi_i(\tau)| \right)$$

where $\xi_i(t)$ is the ith component of $\xi(t)$.

Definition 3: ($\mathcal{L}_1$-norm of a proper linear BIBO system) the $\mathcal{L}_1$-norm of a BIBO stable proper single input/single output (SISO) system is defined as

$$\|H(s)\|_{\mathcal{L}_1} = \int_0^\infty |h(t)|\, \mathrm{d}t$$

where $h(t)$ is the impulse response of $H(s)$.

Lemma 2: For a BIBO stable proper SISO system $H(s)$ with input $u(t)$ and output $y(t)$, we have

$$\|y_t\|_{\mathcal{L}_\infty} \le \|H(s)\|_{\mathcal{L}_1} \|u_t\|_{\mathcal{L}_\infty}, \quad \forall\ t \ge 0$$

B. $\mathcal{L}_1$ Adaptive Output Feedback Controller

The main benefit of the $\mathcal{L}_1$ adaptive controller proposed in this paper is its ability for fast and robust adaptation, which leads to desired transient performance for the system's input and output signals simultaneously, in addition to steady-state tracking. Moreover, analytically computable performance bounds can be derived for the system output as compared with the response of a (minimum-phase) desired model $M(s)$, which is designed to meet the desired specifications, to ensure that

$$q(s) \approx M_q(s) q_c(s), \qquad r(s) \approx M_r(s) r_c(s) \tag{23}$$

In this paper, for simplicity, we restrict ourselves to desired dynamics described by second order systems, yielding

$$M_q(s) = \frac{\omega_{nq}^2}{s^2 + 2\zeta_q \omega_{nq} s + \omega_{nq}^2}, \quad M_r(s) = \frac{\omega_{nr}^2}{s^2 + 2\zeta_r \omega_{nr} s + \omega_{nr}^2}$$
$$\omega_{nq}, \qquad \zeta_q, \qquad \omega_{nr}, \qquad \zeta_r > 0 \tag{24}$$

Since the pitch rate and the yaw rate channels in (14) have the same structure, we define the $\mathcal{L}_1$ adaptive control architecture only for the pitch rate loop. The same analysis can be applied to the yaw rate loop.

In what follows we present the recently developed $\mathcal{L}_1$ output feedback adaptive controller structure in [27], which was derived specifically to deal with nonstrictly positive-real desired models such as the ones in (24). We start by noting that the system

$$q(s) = G_q(s)(q_{\mathrm{ad}}(s) + z_q(s)) \tag{25}$$

can be rewritten in terms of the desired system behavior, defined by $M_q(s)$, as

$$q(s) = M_q(s)(q_{\mathrm{ad}}(s) + \sigma_q(s)) \tag{26}$$

where the uncertainties due to $G_q(s)$ and $z_q(s)$ are lumped in the signal $\sigma_q(s)$, which is defined as

$$\sigma_q(s) = \frac{(G_q(s) - M_q(s)) q_{\mathrm{ad}}(s) + G_q(s) z_q(s)}{M_q(s)} \tag{27}$$

The philosophy behind the $\mathcal{L}_1$ adaptive controller proposed is to introduce separation between adaptation and robustness. The controller obtains the estimate of the uncertainties via a fast estimation scheme and defines the control signal as the output of a low-pass filter, which compensates for the effect of these uncertainties on the system output within the bandwidth of the control channel. This low-pass filter not only guarantees that the control signal stays in the low-frequency range even in the presence of fast adaptation and large reference inputs, but also leads to separation between adaptation and robustness, and defines the trade-off between performance and robustness [28]. Adaptation is based on a piecewise constant adaptive law and uses a state predictor to update the estimate of the uncertainties. The $\mathcal{L}_1$ adaptive control architecture for the pitch rate channel is represented in Fig. 5 and its elements are introduced below:

1) State predictor: let ($A_{m_q} \in \mathbb{R}^{2\times 2}$, $b_{m_q} \in \mathbb{R}^2$, $c_{m_q} \in \mathbb{R}^2$) be the minimal realization of $M_q(s)$ in controllable canonical form, with A_{m_q} being a Hurwitz matrix. Hence, (A_{m_q}, b_{m_q}, $c_{m_q}^\top$) is controllable and observable. Therefore, the system in (26) can be rewritten as

$$\dot{x}_q(t) = A_{m_q} x_q(t) + b_{m_q}(q_{\mathrm{ad}}(t) + \sigma_q(t)), \qquad x_q(0) = 0$$
$$q(t) = c_{m_q}^\top x_q(t) \tag{28}$$

The state predictor is then given by

$$\dot{\hat{x}}_q(t) = A_{m_q} \hat{x}_q(t) + b_{m_q} q_{\mathrm{ad}}(t) + \hat{\sigma}_q(t), \qquad \hat{x}_q(0) = 0$$
$$\hat{q}(t) = c_{m_q}^\top \hat{x}_q(t) \tag{29}$$

where $\hat{\sigma}_q(t) \in \mathbb{R}^2$ is the vector of adaptive estimates. Notice that in the state predictor equations $\hat{\sigma}_q(t)$ appears in an unmatched fashion as opposed to Eq. (28).

2) Adaptive law: let $P_q = P_q^\top > 0$ be the solution to the algebraic Lyapunov equation:

$$A_{m_q}^\top P_q + P_q A_{m_q} = -Q_q, \qquad Q_q = Q_q^\top > 0 \tag{30}$$

From the properties of P_q, it follows that there exists a nonsingular matrix $\sqrt{P_q}$ such that

$$P_q = \sqrt{P_q}^\top \sqrt{P_q}$$

Given the vector $c_{m_q}^\top (\sqrt{P_q})^{-1}$, let D_q be the (1×2), dimensional nullspace of $c_{m_q}^\top (\sqrt{P_q})^{-1}$, i.e.,

$$D_q (c_{m_q}^\top (\sqrt{P_q})^{-1})^\top = 0$$

and let Λ_q be defined as

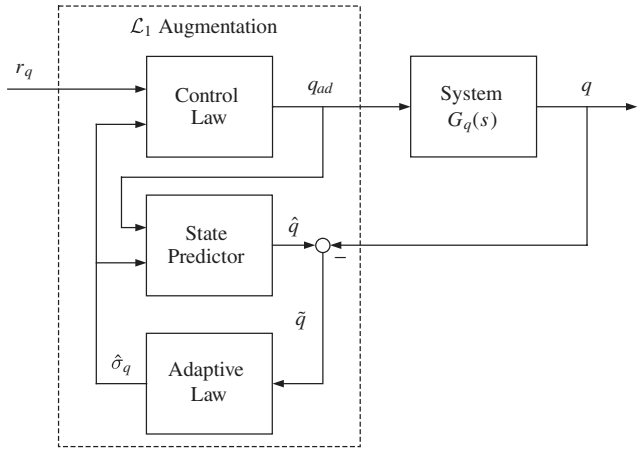

Fig. 5 $\mathcal{L}_1$ adaptive augmentation loop for pitch rate control.

$$\Lambda_q = \begin{bmatrix} c_{m_q}^\top \\ D_q\sqrt{P_q} \end{bmatrix} \in \mathbb{R}^{2\times 2}$$

The update law for $\hat{\sigma}_q(t)$ is defined via the adaptation sampling time $T_s > 0$, which can be related to the available CPU clock frequency, as

$$\begin{aligned} \hat{\sigma}_q(t) &= \hat{\sigma}_q(iT_s), \qquad t \in [iT_s, (i+1)T_s) \\ \hat{\sigma}_q(iT_s) &= -\Phi_q^{-1}(T_s)\mu_q(iT_s) \end{aligned} \tag{31}$$

for $i = 0, 1, 2, \ldots$, where $\Phi_q(T_s)$ is an 2×2 matrix defined as

$$\Phi_q(T_s) = \int_0^{T_s} \mathrm{e}^{\Lambda_q A_{m_q} \Lambda_q^{-1}(T_s-\tau)} \Lambda_q \, \mathrm{d}\tau$$

while

$$\mu_q(iT_s) = e^{\Lambda_q A_{m_q} \Lambda_q^{-1} T_s} 1_1 \tilde{q}(iT_s)$$

with $\tilde{q}(t)$ being defined as $\tilde{q}(t) = \hat{q}(t) - q(t)$, and 1_1 denoting the basis vector in $\mathbb{R}^2$ with its first element equal to one and all other elements being zero.

3) Control law: the control signal is generated by

$$q_{\mathrm{ad}}(s) = C_q(s) r_q(s) - \frac{C_q(s)}{M_q(s)} c_{m_q}^\top (s\mathbb{I} - A_{m_q})^{-1} \hat{\sigma}_q(s) \tag{32}$$

where $r_q(t)$ is a bounded reference input signal with bounded first and second derivatives, and $C_q(s)$ is a strictly proper low-pass filter with $C_q(0) = 1$ ensuring that $\frac{C_q(s)}{M_q(s)} c_{m_q}^\top (s\mathbb{I} - A_{m_q})^{-1}$ is a proper transfer function.

The complete $\mathcal{L}_1$ adaptive output feedback controller consists of (29), (31), and (32), subject to the following stability conditions: the design of $M_q(s)$ and $C_q(s)$ must ensure that

$$H_q(s) = \frac{G_q(s) M_q(s)}{C_q(s) G_q(s) + (1 - C_q(s)) M_q(s)} \tag{33}$$

is stable and that the following $\mathcal{L}_1$-norm condition holds

$$\| H_q(s)(1 - C_q(s)) \|_{\mathcal{L}_1} L_q < 1 \tag{34}$$

where L_q was introduced in Assumption 4.

Next we avail ourselves of previous work on $\mathcal{L}_1$ adaptive control theory to show that if the adaptive sampling time T_s is sufficiently small, then the closed-loop adaptive system is stable and tracks the reference command both in transient and steady state with uniform performance bounds that can be systematically improved by reducing the adaptive sampling time. We refer to [27] for detailed derivations and further details of this result.

To streamline the subsequent analysis, we need to introduce the closed-loop reference system that the $\mathcal{L}_1$ adaptive controller in (29), (31), and (32) tracks both in transient and steady state. To this effect, we consider the ideal nonadaptive version of the adaptive controller and define the auxiliary closed-loop reference system as:

$$q_{\mathrm{ref}}(s) = M_q(s)(q_{\mathrm{ad}_{\mathrm{ref}}}(s) + \sigma_{q_{\mathrm{ref}}}(s)) \tag{35}$$

$$\sigma_{q_{\mathrm{ref}}}(s) = \frac{(G_q(s) - M_q(s)) q_{\mathrm{ad}_{\mathrm{ref}}}(s) + G_q(s) z_q(s)}{M_q(s)} \tag{36}$$

$$q_{\mathrm{ad}_{\mathrm{ref}}}(s) = C_q(s)(r_q(s) - \sigma_{q_{\mathrm{ref}}}(s)) \tag{37}$$

Lemma 3: If $C_q(s)$ and $M_q(s)$ are designed to satisfy the requirements in (33) and (34), then the closed-loop reference system in (35–37) is bounded-input bounded-output (BIBO) stable.

Proof: The proof of this result can be found in [27]. □

Lemma 4: Given the closed-loop system of the plant in (25) with the $\mathcal{L}_1$ adaptive controller defined via (29–32), subject to the stability requirements in (33) and (34), if

$$\| r_{qt} \|_{\mathcal{L}_\infty} \leq \gamma_{r_q}$$

then

$$\| (q - q_{\mathrm{ref}})_t \|_{\mathcal{L}_\infty} \leq \gamma_q, \qquad \| (q_{\mathrm{ad}} - q_{\mathrm{ad}_{\mathrm{ref}}})_t \|_{\mathcal{L}_\infty} \leq \gamma_{q_{\mathrm{ad}}} \tag{38}$$

with

$$\lim_{T_s \to 0} \gamma_q = 0, \qquad \lim_{T_s \to 0} \gamma_{q_{\mathrm{ad}}} = 0$$

Proof: The proof of this result can be found in [27]. □

It follows from Lemma 4 that the bounds on the difference between the input and the output signals of the closed-loop adaptive system and the closed-loop reference system, $q(t) - q_{\mathrm{ref}}(t)$ and $q_{\mathrm{ad}}(t) - q_{\mathrm{ad}_{\mathrm{ref}}}(t)$, can be rendered arbitrarily small by reducing the adaptive sampling time. We notice, however, that the choice of small T_s may be limited by hardware.

We note that the control law $q_{\mathrm{ad}_{\mathrm{ref}}}(t)$ in the closed-loop reference system, which is used in the analysis of $\mathcal{L}_\infty$-norm bounds, is not implementable since its definition involves the system uncertainties. Lemma 4 ensures that the $\mathcal{L}_1$ adaptive controller approximates $q_{\mathrm{ad}_{\mathrm{ref}}}(t)$ both in transient and steady state. So it is important to understand how the performance bounds in (38) can be used for ensuring uniform transient response with desired specifications. We notice that the following ideal control signal $q_{\mathrm{ad}_{\mathrm{id}}}(t) = r_q(t) - \sigma_q(t)$ is the one that leads to desired system response:

$$q_{\mathrm{id}}(s) = M_q(s) r_q(s) \tag{39}$$

by canceling the uncertainties exactly. Thus, the reference system in (35–37) has a different response as compared with (39). In [8], specific design guidelines are suggested for the selection of the low-pass filter in the control law that lead to the desired system response. A similar reasoning can be applied in the case of the architecture proposed in this paper.

Lemma 5: Given the $\mathcal{L}_1$ adaptive controller defined via (29–32) subject to the stability requirements in (33) and (34), if

$$\| r_{qt} \|_{\mathcal{L}_\infty} \leq \gamma_{r_q}, \qquad \| \dot{r}_{qt} \|_{\mathcal{L}_\infty} \leq \gamma_{\dot{r}_q}, \qquad \| \ddot{r}_{qt} \|_{\mathcal{L}_\infty} \leq \gamma_{\ddot{r}_q} \tag{40}$$

and also the initial condition verifies

$$\| [\, q(0) - r_q(0), \quad \dot{q}(0) - \dot{r}_q(0) \,]^\top \| < \frac{2\|P_q b_{m_q}\|}{\lambda_{\min}(Q_q)} (2\zeta_q \omega_{nq} \gamma_{\dot{r}_q} + \gamma_{\ddot{r}_q}) \tag{41}$$

then it follows that

$$\| (q - r_q)_t \|_{\mathcal{L}_\infty} \leq \gamma_\theta \triangleq \gamma_q + \bar{\gamma}_q + \frac{2\|P_q b_{m_q}\|}{\lambda_{\min}(Q_q)} (2\zeta_q \omega_{nq} \gamma_{\dot{r}_q} + \gamma_{\ddot{r}_q}) \tag{42}$$

with

$$\lim_{T_s \to 0} \gamma_q = 0, \qquad \lim_{C_q(s) \to 1} \bar{\gamma}_q = 0$$

Proof: The proof of this result, which uses some of the derivations and results in Lemma 4, is given in the Appendix. □

Similarly, if we implement the $\mathcal{L}_1$ adaptive controller for the system

$$r(s) = G_r(s)(r_{\mathrm{ad}}(s) + z_r(s))$$

subject to

$$\| r_{rt} \|_{\mathcal{L}_\infty} \leq \gamma_{r_r}, \qquad \| \dot{r}_{rt} \|_{\mathcal{L}_\infty} \leq \gamma_{\dot{r}_r}, \qquad \| \ddot{r}_{rt} \|_{\mathcal{L}_\infty} \leq \gamma_{\ddot{r}_r}$$

and also to

$$\|[\, r(0) - r_r(0), \quad \dot{r}(0) - \dot{r}_r(0)\,]^\top\| < \frac{2\|P_r b_{m_r}\|}{\lambda_{\min}(Q_r)}(2\zeta_r\omega_{nr}\gamma_{\dot{r}_r} + \gamma_{\ddot{r}_r}) \tag{43}$$

it is possible to show that

$$\|(r - r_r)_t\|_{\mathcal{L}_\infty} \le \gamma_\psi \tag{44}$$

with $\gamma_\psi > 0$ being a constant similar to γ_θ.

If we want to further reduce the bounds γ_θ and γ_ψ, we need to choose a small adaptive sampling time T_s and a high bandwidth of the low-pass filters $C_q(s)$ and $C_r(s)$. A decrease in the adaptive sampling time T_s requires a higher frequency clock of the CPU, while an increase of the bandwidth of the low-pass filter will sacrifice the robustness of the system, as the choice of the low-pass filter defines the trade-off between performance and robustness.

C. Path-Following Closed-Loop Dynamics

At this point, the point-mass assumption in Sec. III is removed and stability of the cascaded closed-loop system with the UAV dynamics, the $\mathcal{L}_1$ adaptive augmentation, and the outer-loop path-following algorithm shown in Fig. 4 is discussed. First, we show that the outer-loop path-following commands $q_c(t)$ and $r_c(t)$ and their first and second derivatives are bounded, which in turn allows us to prove that the original domain of attraction for the kinematic-error equations given in (21) becomes a positively invariant set for the complete path-following system. The uniform performance bounds that the $\mathcal{L}_1$ adaptive controller guarantees both in transient and steady state are critical to prove this result.

Remark 4: Stability of the path-following closed-loop dynamics with the $\mathcal{L}_1$ augmentation loop, which is the main result of the paper, is proven in two steps:

1) In Lemma 6, we show that if the path-following kinematic-error vector $x(\tau)$ remains within the set Ω, defined in (21), for all time $\tau \in [0, t]$, then the outer-loop path-following commands $q_c(t)$ and $r_c(t)$ and their first and second derivatives are bounded. In particular, we first show that using the bounds on the path-following kinematic errors, the path-following commands $q_c(\tau)$ and $r_c(\tau)$ are bounded for all $\tau \in [0, t]$. Then, these bounds together with the results of Lemmas 3 and 4 are used to derive the bounds for the first and second derivatives of $q_c(\tau)$ and $r_c(\tau)$ for all $\tau \in [0, t]$.

2) Using the results in Lemma 6, we show in Theorem 1 that if the initial path-following kinematic-error vector $x(0)$ belongs to the set Ω, then the outer-loop path-following controller with the $\mathcal{L}_1$ adaptive augmentation can be designed so that the path-following kinematic-error vector $x(t)$ remains inside the set Ω for all time $t \ge 0$. The proof of this result is done by contradiction, and requires the use of truncated $\mathcal{L}_\infty$-norms (see Definition 2).

Lemma 6: If $x(\tau) \in \bar{\Omega}$ for all $\tau \in [0, t]$, where $\bar{\Omega}$ is the closure of the set Ω, defined in (21), the initial conditions verify (41) and (43), and moreover the design of the $\mathcal{L}_1$ adaptive controller is such that the results of Lemma 3 hold both for the pitch and the yaw channels, then the outer-loop path-following commands $q_c(\tau)$ and $r_c(\tau)$ and their derivatives $\dot{q}_c(\tau)$, $\dot{r}_c(\tau)$, $\ddot{q}_c(\tau)$, and $\ddot{r}_c(\tau)$ are bounded, that is

$$\begin{aligned} &\|q_{ct}\|_{\mathcal{L}_\infty} \le \gamma_{q_c}, \qquad \|\dot{q}_{ct}\|_{\mathcal{L}_\infty} \le \gamma_{\dot{q}_c}, \qquad \|\ddot{q}_{ct}\|_{\mathcal{L}_\infty} \le \gamma_{\ddot{q}_c} \\ &\|r_{ct}\|_{\mathcal{L}_\infty} \le \gamma_{r_c}, \qquad \|\dot{r}_{ct}\|_{\mathcal{L}_\infty} \le \gamma_{\dot{r}_c}, \qquad \|\ddot{r}_{ct}\|_{\mathcal{L}_\infty} \le \gamma_{\ddot{r}_c} \end{aligned} \tag{45}$$

for some positive constants γ_{q_c}, $\gamma_{\dot{q}_c}$, $\gamma_{\ddot{q}_c}$, γ_{r_c}, $\gamma_{\dot{r}_c}$, and $\gamma_{\ddot{r}_c}$.

Proof: The proof is given in the Appendix. □

Next, we define $u_\theta(t)$ and $u_\psi(t)$ as

$$\begin{bmatrix} u_\theta(t) \\ u_\psi(t) \end{bmatrix} = D(t, \theta_e, \psi_e) + T(t, \theta_e)\begin{bmatrix} q(t) \\ r(t) \end{bmatrix} \tag{46}$$

and therefore from (11), one gets

$$\dot{\theta}_e(t) = u_\theta(t) \quad \text{and} \quad \dot{\psi}_e(t) = u_\psi(t) \tag{47}$$

It now follows from (19) and (46) that

$$\begin{bmatrix} u_\theta(t) - u_{\theta_c}(t) \\ u_\psi(t) - u_{\psi_c}(t) \end{bmatrix} = T(t, \theta_e)\begin{bmatrix} q(t) - q_c(t) \\ r(t) - r_c(t) \end{bmatrix} \tag{48}$$

Furthermore, we define γ_{u_θ} and γ_{u_ψ} as

$$\gamma_{u_\theta} = \gamma_\theta + \gamma_\psi, \qquad \gamma_{u_\psi} = \frac{1}{\cos\nu_1}(\gamma_\theta + \gamma_\psi) \tag{49}$$

with γ_θ and γ_ψ being the bounds in (42) and (44) for $r_q(t) \equiv q_c(t)$ and $r_r(t) \equiv r_c(t)$.

Theorem 1: Let the progression of point P along the path be governed by (18). For any smooth $v(t)$ verifying (13), if

1) The initial path-following state vector satisfies

$$x(0) \in \Omega$$

2) The initial pitch and yaw rates verify

$$\|[\, q(0) - r_q(0), \quad \dot{q}(0) - \dot{r}_q(0)\,]^\top\| < \frac{2\|P_q b_{m_q}\|}{\lambda_{\min}(Q_q)}(2\zeta_q\omega_{nq}\gamma_{\dot{r}_q} + \gamma_{\ddot{r}_q}) \tag{50}$$

$$\|[\, r(0) - r_r(0), \quad \dot{r}(0) - \dot{r}_r(0)\,]^\top\| < \frac{2\|P_r b_{m_r}\|}{\lambda_{\min}(Q_r)}(2\zeta_r\omega_{nr}\gamma_{\dot{r}_r} + \gamma_{\ddot{r}_r}) \tag{51}$$

where $\gamma_{\dot{q}_c}$, $\gamma_{\ddot{q}_c}$, $\gamma_{\dot{r}_c}$ and $\gamma_{\ddot{r}_c}$ were introduced in (45).

3) T_s is chosen to be sufficiently small, while $M_q(s)$, $C_q(s)$, $M_r(s)$, and $C_r(s)$ are designed to verify

$$\gamma_{u_\theta} + \gamma_{u_\psi} \le \frac{\sqrt{cc_2}}{2}\frac{\lambda_{\min}(Q_{\text{pf}})}{\lambda_{\max}(P_{\text{pf}})} \tag{52}$$

where P_{pf} was introduced in (22), Q_{pf} is given by

$$Q_{\text{pf}} = \text{diag}\left(\frac{K_1}{c_1}, \ \frac{v_{\min}\cos\nu_1}{c_1(d+d_2)}, \ \frac{v_{\min}}{c_1(d+d_1)}, \ \frac{K_2}{c_2}, \ \frac{K_3}{c_2}\right) \tag{53}$$

and γ_{u_θ} and γ_{u_ψ} were defined in (49), then $x(t) \in \Omega$ for all $t \ge 0$, that is

$$V_{\text{pf}}(x(t)) < \frac{c}{2}, \quad \forall\ t \ge 0 \tag{54}$$

and thus the complete closed-loop cascaded system is ultimately bounded.

Proof: The proof is given in the Appendix. □

Remark 5: We notice that the above stability proof is different from common backstepping-type analysis for cascaded systems. The advantage of the above structure for the feedback design is that it retains the properties of the autopilot, which is designed to stabilize the UAV. As a result, it leads to ultimate boundedness instead of asymptotic stability.

V. Flight Test Results

This section presents flight test results for the real-time implementation of the path-following control system with the $\mathcal{L}_1$ adaptive augmentation loop shown in Fig. 4. These results demonstrate the applicability of the path-following control architecture developed in this paper to small UAVs, and illustrate the benefits of the proposed framework. In particular, the flight tests show significant improvement in path-following performance when a commercial AP is augmented with an $\mathcal{L}_1$ adaptive controller. The discussion in this section also gives practical insight into the process of tuning the $\mathcal{L}_1$-augmented control system.

The path-following control algorithm with the $\mathcal{L}_1$ augmentation was implemented on an experimental UAV Rascal operated by NPS, and thoroughly tested in hardware in the loop (HIL) simulations and in numerous flights at Camp Roberts, CA. The payload bay of the aircraft was used to house the Piccolo Plus autopilot and a PC104 embedded computer running the algorithms in real-time at 100 Hz, while communicating with the autopilot over a full duplex serial link at 20 Hz. The main command and control link of the autopilot [29] is

not used in the experiment but preserved for safety reasons. Instead, the onboard avionics were augmented with a wireless mesh communication link to allow for real-time control, tuning, and performance monitoring of the developed software. In particular, this link is used to (bidirectionally) exchange telemetry data in real time between the autopilot and the ground station. The content includes positional, velocity, acceleration, and rates data of the standard telemetry and control messages of the Piccolo communication protocol. The experimental setup is shown in Fig. 6. The main benefit of this configuration relies on two primary facts. First, the control code resides onboard and directly communicates with the inner-loop controller therefore eliminating any communications delays and dropouts. Second, both the HIL architecture and the actual flight setup, including any possible online modification of the control system parameters, are identical. This allows for a seamless transition from the simulation environment to the flight tests. More details on the architecture of the developed flight test system and its current applications can be found in [30].

The actual implementation of the path-following controller with the $\mathcal{L}_1$ augmentation loop is practically the same as the one shown in Figs. 4 and 5 except for the fact that two logical switches were added to allow for separate tuning of the outer-loop path-following control algorithm and the $\mathcal{L}_1$ adaptive augmentation loop.

Tuning of the control system parameters is done in HIL and consists of four key sequential steps: 1) adjustment of the AP gains so as to guarantee required tracking performance of the (manually) issued angular-rate commands while operating in the low angle of attack and sideslip angle range, 2) system identification (SID) experiment, which provides estimates of the maximum allowable body rates and limits on the bandwidths of $M(s)$ and $C(s)$ for each control channel, 3) tuning of the outer-loop kinematic controller, and 4) tuning of the $\mathcal{L}_1$ adaptive augmentation.

The SID experiment consists of the identification of the UAV dynamics in response to a predefined set of doublet commands in the lateral and the longitudinal channels. Typically, a sequence of symmetric aileron (rudder) and elevator (throttle) doublets for the lateral and longitudinal channels, respectively, is executed. A new capability of the Piccolo Plus autopilot allowed for data sampling in SID experiment at 100 Hz, covering the range of natural frequencies of the small UAV.

Next, the parameters of the path-following kinematic algorithm defined in (19) and (20) are adjusted, and performance of the nominal system (without the $\mathcal{L}_1$ augmentation) is evaluated in HIL simulations. This step uses the same rules of conventional PID tuning. The main criteria considered are the path-following errors and the angular-rate tracking errors.

Then, the same flight conditions, outer-loop kinematic algorithm, and AP gains are used to tune the $\mathcal{L}_1$ adaptive augmentation. Initial guesses of the adaptation sampling time T_s, and the bandwidths of $M(s)$ and $C(s)$ can be estimated based on the following considerations: the bandwidth of each control loop of the AP was suggested by the SID experiment, resulting, for example, in an initial filter bandwidth of 0.6 $\frac{\text{rad}}{\text{s}}$ for the turn-rate channel, while the desired system $M(s)$ was chosen to be slightly slower than $C(s)$, with a bandwidth of 0.5 $\frac{\text{rad}}{\text{s}}$. The lower bound on the adaptation sampling time $T_s = \frac{1}{85}$ s was estimated based on the results in [27], using $T_s = \frac{1}{100}$ s for the implementation. Taking these values as a starting point, the tuning of the $\mathcal{L}_1$ adaptive controller was done in two steps by analyzing the internal signals of the augmentation system: the estimation error $\tilde{y}(t)$, the adaptive estimate $\hat{\sigma}(t)$, and the $\mathcal{L}_1$ contribution to the control signal. For the chosen adaptation sampling time $T_s = \frac{1}{100}$ s, the tuning of the reference system $M(s)$ minimizes the estimation error and results in a high-frequency limited-amplitude adaptive estimate. At the second step, the bandwidth of the low-pass filter $C(s)$ in the control law (32) was gradually adjusted to achieve the desired tracking performance, effectively suppressing the high-frequency oscillations in the control signal and providing robust tracking. After a series of HIL simulations, the following parameters of the $\mathcal{L}_1$ controller were obtained:

$$M(s) = \frac{0.55^2}{s^2 + 2\ 0.95\ 0.55 s + 0.55^2}, \qquad C(s) = \frac{0.62}{s + 0.62}\frac{5}{s+5}$$
$$T_s = 0.01 \text{ s}$$

It is important to note also that, unlike conventional adaptive controllers, the systematic design procedures of the $\mathcal{L}_1$ adaptive control theory significantly reduce the tuning effort required to achieve desired closed-loop performance, which in turn facilitates the transition of the path-following control architecture from the simulation environment to real flight tests.

In the remaining of the section, we present some of the flight test results obtained at Camp Roberts, CA. First, however, we need to introduce and provide some details about the procedure followed during the flight experiment. Initially, while the UAV is flying in conventional waypoint navigation mode, a switch request is sent from the ground station to the UAV over a wireless link. Together with this request, the desired final conditions (Fin.C.) for the path and the control parameters for the outer-loop path-following controller and the $\mathcal{L}_1$ augmentation loop are also transmitted to the UAV. Upon receipt of this initialization signal, the UAV states are captured as initial path conditions (I.C.), which, along with the Fin.C., provide

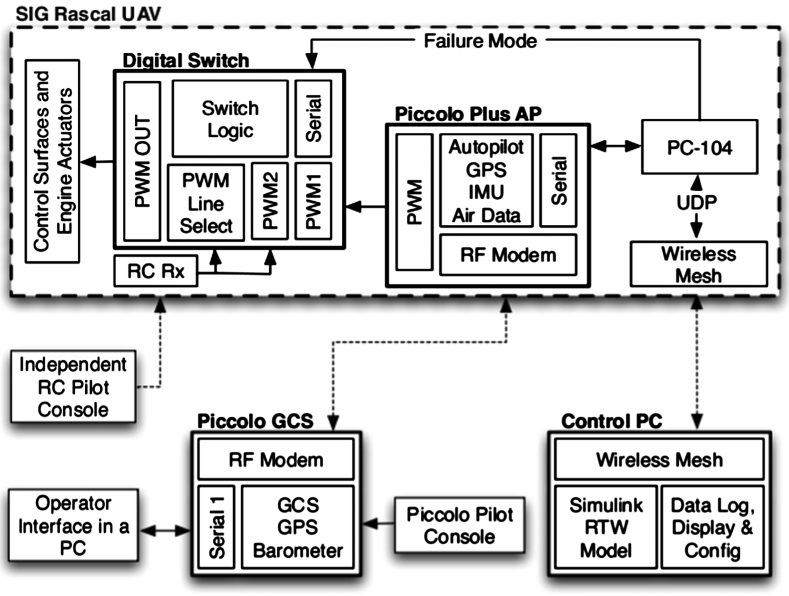

Fig. 6 Avionics architecture.

boundary conditions for the path generation algorithm. After the path is (locally) generated, the UAV starts operating in path-following mode, and from that moment on, it tracks the path until it arrives at the final point, upon which it can be either automatically stopped, transferring the UAV to the standard AP control mode, or new final conditions can be automatically specified allowing for the experiment to be continued. While in flight, the onboard system continuously logs and transmits UAV telemetry and controller data to the ground, which is essential for real-time monitoring of the control system.

Flight test results showing the applicability of the developed control architecture, and comparing the performance of the path-following algorithm with and without $\mathcal{L}_1$ adaptation are shown in Fig. 7. The flight test data include the 2-D projection of the commanded and actual paths, the commanded $r_c(t)$ and measured $r(t)$ turn-rate responses, and the path tracking errors $y_F(t)$ and $z_F(t)$

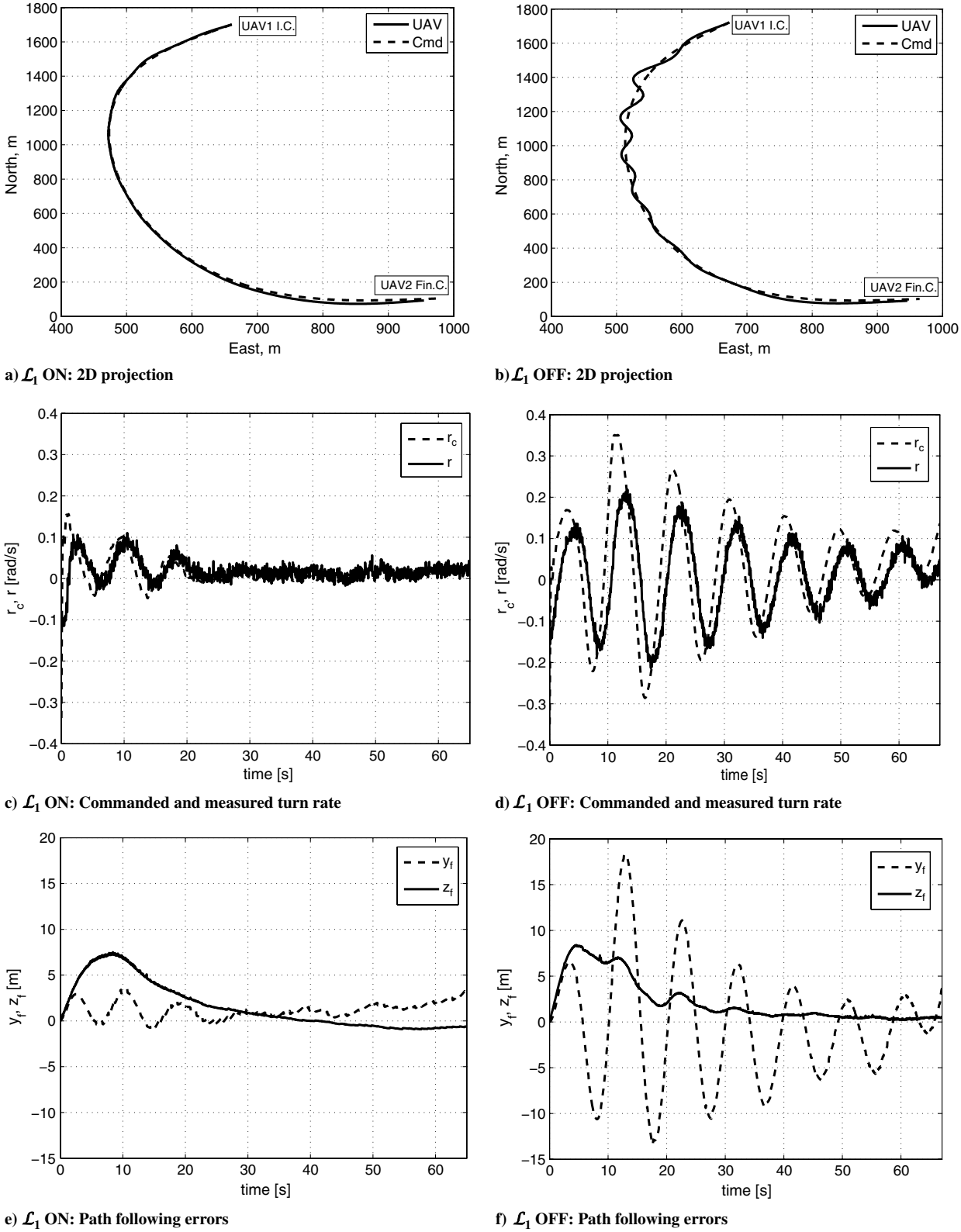

a) $\mathcal{L}_1$ ON: 2D projection

b) $\mathcal{L}_1$ OFF: 2D projection

c) $\mathcal{L}_1$ ON: Commanded and measured turn rate

d) $\mathcal{L}_1$ OFF: Commanded and measured turn rate

e) $\mathcal{L}_1$ ON: Path following errors

f) $\mathcal{L}_1$ OFF: Path following errors

Fig. 7 Fight Test. Path-following performance with and without $\mathcal{L}_1$ adaptive augmentation.

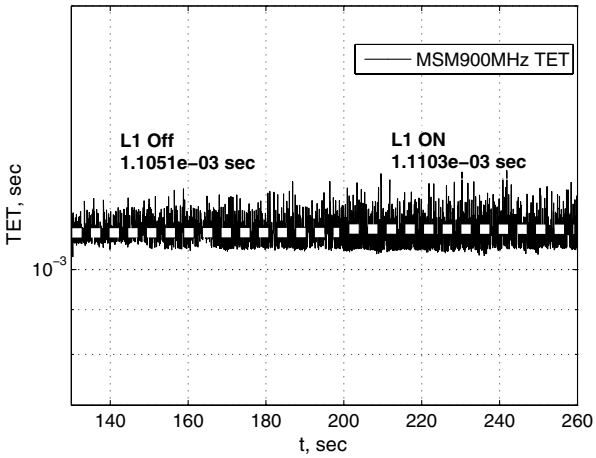

Fig. 8 HIL. Task execution time: negligible increase in CPU load.

resolved in the parallel transport frame. In these experiments, the speed command was fixed at 25 $\frac{\text{m}}{\text{s}}$, and the bank angle was limited to 25 deg, which results in about 0.2 $\frac{\text{rad}}{\text{s}}$ turn-rate capability that in fact enables tracking of much more aggressive paths (with radii of curvature up to 136 m) than the one presented in the figure. Results show that the UAV is able to follow the path, keeping the path-following tracking errors reasonably small during the whole experiment. The plots also show improved path-following performance when the $\mathcal{L}_1$ augmentation loop is enabled. On the one hand, the nominal outer-loop path-following controller exhibits significant oscillatory behavior, with rate commands going up to 0.35 rad/s and with maximum path tracking errors around 18 m. On the other hand, when the $\mathcal{L}_1$ augmentation loop is active, the rate commands do not exceed 0.15 rad/s, which results, in turn, in less than 8 m of path tracking errors. Therefore, the presence of fast adaptation improves the angular-rate tracking capabilities of the inner-loop controller, which results in improved path-following capabilities with reduced oscillations. At this point it is important to note that the adaptive controller does not introduce any high-frequency content into the commanded turn-rate signal, as it can be seen by comparing Figs. 7c and 7d. In fact, the oscillations present in both the control signal and the actual turn rate are due to turbulence, and one can see that the amplitude of these oscillations is similar in both figures. Also, there should not be any confusion with the data presented in the plots: while the time scale of the flight experiments is measured in tens of seconds, the data sampling rate is high (20 Hz). As a result, the oscillations due to turbulence might give the impression that the signals, in particular the control commands, have high-frequency content, which is not the case.

In addition to these flight test results, we have analyzed in HIL simulation the computational complexity of the algorithms developed. Figure 8 shows the computational load required to implement in real-time 1) the outer-loop path-following controller, and 2) the same outer-loop controller with the $\mathcal{L}_1$ augmentation loop. The parameter chosen to represent the computational load is an average task execution time (TET), which is the time required to execute the entire control code during one base sample interval ($\frac{1}{100}$ s). The control code was implemented onboard of an MSM900BEV[§§] industrial PC104 computer using xPC/RTW target[¶¶] development environment. This figure highlights two important points: first, the average TET ($\approx$0.001 s) is an order of magnitude less than the base sampling time of the real-time code (0.01 s), which implies that the sampling time T_s of the real-time code implementation was chosen quite conservatively and could be reduced to improve the closed-loop performance; and second, the difference in the required CPU load when the adaptive controller is enabled or disabled is negligible (an additional 0.052% with respect to the nominal controller), which suggests its easy implementation in any application.

Finally, we note that the achieved functionality of a small UAV following 3-D curves in inertial space has never been available for airplanes equipped with traditional autopilots designed to provide waypoint navigation only. This fact alone significantly extends the range of possible applications of (small) UAVs. The $\mathcal{L}_1$ augmentation loop is introduced to improve the stability robustness and performance of the vehicle in the presence of uncertainties, control surface failures, structural damage, and environmental disturbances. Moreover, the performance bounds that the $\mathcal{L}_1$ adaptive controller guarantees are critical to prove stability of the overall path-following closed-loop system.

VI. Conclusions

A novel solution was presented to the problem of path-following control of UAVs. The solution proposed leads to an inner-outer control structure that exploits the availability of commercial autopilots for angular-rate command tracking. The theoretical framework adopted relies on a nonlinear control strategy derived at a kinematic level for path following in 3-D space, along with an $\mathcal{L}_1$ adaptive output feedback controller augmenting the existing autopilot. The $\mathcal{L}_1$ adaptive augmentation strategy was introduced to meet strict performance requirements in the presence of modeling uncertainties and environmental disturbances, effectively allowing to cope with the UAV and autopilot dynamics. The adopted architecture outperforms the functionality of the conventional waypoint navigation method, enabling a UAV with an off-the-shelf autopilot to follow a predetermined path that it was not otherwise designed to follow. Both theoretical and practical aspects of the problem were addressed. Flight test results showed the effectiveness of the framework adopted for UAV path following.

Appendix: Proofs

Proof of Lemma 1: If $q(t) \equiv q_c(t)$ and $r(t) \equiv r_c(t)$, it is easy to check from (11) and (19) that

$$\dot{\theta}_e(t) = u_{\theta_c}(t), \qquad \dot{\psi}_e(t) = u_{\psi_c}(t)$$

Then, it follows from (11) and (18) and the path-following control laws in (19) and (20) that

$$\begin{aligned}
\dot{V}_{\text{pf}} &= \frac{x_F}{c_1}(-\dot{\ell}(1-k_1(\ell)y_F - k_2(\ell)z_F) + v\cos\theta_e\cos\psi_e) \\
&\quad + \frac{y_F}{c_1}(-\dot{\ell}k_1(\ell)x_F + v\cos\theta_e\sin\psi_e) + \frac{z_F}{c_1}(-\dot{\ell}k_2(\ell)x_F \\
&\quad - v\sin\theta_e) + \frac{\theta_e-\delta_\theta}{c_2}(u_{\theta_c}-\dot{\delta}_\theta) + \frac{\psi_e-\delta_\psi}{c_2}(u_{\psi_c}-\dot{\delta}_\psi) \\
&= \frac{-x_F(\dot{\ell}-v\cos\theta_e\cos\psi_e)}{c_1} + \frac{y_F v\cos\theta_e\sin\psi_e}{c_1} - \frac{z_F v\sin\theta_e}{c_1} \\
&\quad - \frac{K_2}{c_2}(\theta_e-\delta_\theta)^2 - \frac{K_3}{c_2}(\psi_e-\delta_\psi)^2 + \frac{vz_F(\sin\theta_e-\sin\delta_\theta)}{c_1} \\
&\quad - \frac{vy_F\cos\theta_e(\sin\psi_e-\sin\delta_\psi)}{c_1}
\end{aligned}$$

thus leading to

$$\begin{aligned}
\dot{V}_{\text{pf}} &= -\frac{K_1}{c_1}x_F^2 - \frac{K_2}{c_2}(\theta_e-\delta_\theta)^2 - \frac{K_3}{c_2}(\psi_e-\delta_\psi)^2 \\
&\quad + \frac{vy_F\sin\delta_\psi\cos\theta_e}{c_1} - \frac{vz_F\sin\delta_\theta}{c_1}
\end{aligned}$$

Using the definition of the shaping functions $\delta_\theta(t)$ and $\delta_\psi(t)$ in (12) yields

[§§]Advanced digital logic (ADL) | PC104+ : AMD geode LX900 CPU 500 MHz–MSM900BEV.

[¶¶]xPCTarget—perform real-time rapid prototyping and hardware-in-the-loop simulation using PC hardware—simulink. Data available at http://www.mathworks.com/products/xpctarget/.

$$\dot{V}_{\rm pf} = -\frac{K_1}{c_1}x_F^2 - \frac{K_2}{c_2}(\theta_e - \delta_\theta)^2 - \frac{K_3}{c_2}(\psi_e - \delta_\psi)^2 - \frac{v z_F^2}{c_1(|z_F| + d_1)} - \frac{v y_F^2 \cos\theta_e}{c_1(|y_F| + d_2)}$$

and therefore

$$\dot{V}_{\rm pf}(x) = -x^\top Q_{\rm pf} x$$

with

$$Q_{\rm pf} = {\rm diag}\left(\tfrac{K_1}{c_1},\ \tfrac{v\cos\theta_e}{c_1(|y_F|+d_2)},\ \tfrac{v}{c_1(|z_F|+d_1)},\ \tfrac{K_2}{c_2},\ \tfrac{K_3}{c_2}\right) \tag{A1}$$

Letting $d = \sqrt{cc_1}$, where c and c_1 were introduced in (17), we note that over the compact set Ω the following upper bounds hold

$$|x_F(t)| < d, \qquad |y_F(t)| < d, \qquad |z_F(t)| < d$$
$$|\theta_e(t)| < \sqrt{cc_2} + |\delta_\theta(t)| < \sqrt{cc_2} + \sin^{-1}\left(\frac{d}{d+d_1}\right) = \nu_1 < \frac{\pi}{2}$$
$$|\psi_e(t)| < \sqrt{cc_2} + |\delta_\psi(t)| < \sqrt{cc_2} + \sin^{-1}\left(\frac{d}{d+d_2}\right) = \nu_2 < \frac{\pi}{2} \tag{A2}$$

Next, it follows from (A1) and (A2) that $Q_{\rm pf} \geq \bar{Q}_{\rm pf}$, where

$$\bar{Q}_{\rm pf} = {\rm diag}\left(\tfrac{K_1}{c_1},\ \tfrac{v_{\min}\cos\nu_1}{c_1(d+d_2)},\ \tfrac{v_{\min}}{c_1(d+d_1)},\ \tfrac{K_2}{c_2},\ \tfrac{K_3}{c_2}\right) \tag{A3}$$

Since $\bar{Q}_{\rm pf} > 0$ and

$$\dot{V}_{\rm pf}(x) \leq -x^\top \bar{Q}_{\rm pf} x, \quad \forall\ t \geq 0$$

$x(t)$ converges exponentially to zero for all the initial conditions inside the compact set Ω. It then follows from the definitions in (12) that both $\delta_\theta(t)$ and $\delta_\psi(t)$ converge exponentially to zero, and, therefore, $\theta_e(t)$ and $\psi_e(t)$ also converge exponentially to zero, which completes the proof. □

Proof of Lemma 5: If the first bound in (40) holds, then Lemmas 3 and 4 ensure that

$$\|(q - q_{\rm ref})_t\|_{\mathcal{L}_\infty} \leq \gamma_q \tag{A4}$$

with

$$\lim_{T_s \to 0} \gamma_q = 0 \tag{A5}$$

Also, from the definition of the closed-loop reference system in (35–37) and the desired system response in (39) it follows that

$$q_{\rm ref}(s) - q_{\rm id}(s) = (H_q(s)C_q(s) - M_q(s))r_q(s) + H_q(s)(1 - C_q(s))z_q(s)$$

and therefore we have the following upper bound

$$\|(q_{\rm ref} - q_{\rm id})_t\|_{\mathcal{L}_\infty} \leq \|H_q(s)C_q(s) - M_q(s)\|_{\mathcal{L}_1}\gamma_{r_q} + \|H_q(s)(1 - C_q(s))\|_{\mathcal{L}_1}\|z_{qt}\|_{\mathcal{L}_\infty}$$

Assumption 4, together with the results of Lemmas 3 and 4, leads to

$$\|z_{qt}\|_{\mathcal{L}_\infty} \leq L_q\left(\frac{\|H_q(s)C_q(s)\|_{\mathcal{L}_1}\gamma_{r_q} + \|H_q(s)(1 - C_q(s))\|_{\mathcal{L}_1}L_{q_0}}{1 - \|H_q(s)(1 - C_q(s))\|_{\mathcal{L}_1}L_q} + \gamma_q\right) + L_{q0} \triangleq B_{z_q} < \infty$$

and hence it follows that

$$\|(q_{\rm ref} - q_{\rm id})_t\|_{\mathcal{L}_\infty} \leq \bar{\gamma}_q \triangleq \|H_q(s)C_q(s) - M_q(s)\|_{\mathcal{L}_1}\gamma_{r_q} + \|H_q(s)(1 - C_q(s))\|_{\mathcal{L}_1}B_{z_q} \tag{A6}$$

From the definition of $H_q(s)$ in (33), we have

$$\lim_{C_q(s)\to 1} H_q(s)C_q(s) = M_q(s)$$

and therefore we can conclude that

$$\lim_{C_q(s)\to 1} \bar{\gamma}_q = 0 \tag{A7}$$

Finally, letting $e_q(\tau)$ be defined as

$$e_q(\tau) = [\, r_q(\tau) - y_{\rm id}(\tau), \quad \dot{r}_q(\tau) - \dot{q}_{\rm id}(\tau)\,]^\top$$

it follows from the desired response in (39) that

$$\dot{e}_q(\tau) = A_{m_q}e_q(\tau) + b_{m_q}(\ddot{r}_q(\tau) + 2\zeta_q\omega_{nq}\dot{r}_q(\tau))$$

Consider now the Lyapunov function candidate

$$V_e(e_q(\tau)) = e_q^\top(\tau)P_q e_q(\tau)$$

where P_q was introduced in (30). Then,

$$\dot{V}_e(\tau) = -e_q^\top(\tau)P_q e_q(\tau) + 2e_q^\top(\tau)P_q b_{m_q}(\ddot{r}_q(\tau) + 2\zeta_q\omega_{nq}\dot{r}_q(\tau))$$

which leads to the following upper bound:

$$\dot{V}_e(\tau) \leq -\lambda_{\min}(Q_q)\|e_q(\tau)\|^2 + 2\|e_q(\tau)\|\|P_q b_{m_q}\||\ddot{r}_q(\tau) + 2\zeta_q\omega_{nq}\dot{r}_q(\tau)| \tag{A8}$$

Then, if the bounds on the first and second derivatives of the reference signal $r_q(t)$ in (40) hold and the initial condition verifies (41), it is easy to check that

$$\|e_q(\tau)\| \leq \frac{2\|P_q b_{m_q}\|}{\lambda_{\min}(Q_q)}(\gamma_{\dot{r}_q} + 2\zeta_q\omega_{nq}\gamma_{\dot{r}_q}), \quad \forall\ \tau \in [0, t]$$

which implies that

$$\|(r_q - q_{\rm id})_t\|_{\mathcal{L}_\infty} \leq \frac{2\|P_q b_{m_q}\|}{\lambda_{\min}(Q_q)}(\gamma_{\dot{r}_q} + 2\zeta_q\omega_{nq}\gamma_{\dot{r}_q})$$

Consequently, it follows from the bounds in (A4), (A6), and (A8) that a straightforward upper bound for $r_q(t) - q(t)$ is given by

$$\|(r_q - q)_t\|_{\mathcal{L}_\infty} \leq \gamma_q + \bar{\gamma}_q + \frac{2\|P_q b_{m_q}\|}{\lambda_{\min}(Q_q)}(\gamma_{\dot{r}_q} + 2\zeta_q\omega_{nq}\gamma_{\dot{r}_q})$$

This bound, together with the limiting relations (A5) and (A7), proves the claim in the Lemma. □

Proof of Lemma 6: Let $d = \sqrt{cc_1}$. We recall from Lemma 1 that, if $x(\tau) \in \bar{\Omega}$ for all $\tau \in [0, t]$, then one finds that

$$|x_F(\tau)| \leq d \qquad |y_F(\tau)| \leq d \qquad |z_F(\tau)| \leq d$$
$$|\theta_e(\tau)| \leq \nu_1 \qquad |\psi_e(\tau)| \leq \nu_2 \tag{A9}$$

and also that

$$|\theta_e(\tau) - \delta_\theta(\tau)| \leq \sqrt{cc_2}, \qquad |\psi_e(\tau) - \delta_\psi(\tau)| \leq \sqrt{cc_2} \tag{A10}$$

which hold for any $\tau \in [0, t]$.

From the feasibility of the path we can conclude that both $k_1(\ell)$ and $k_2(\ell)$, as well as their partial derivatives with respect to the path length ℓ, are bounded. Then, it follows from (13) and (A9) that the rate of progression $\dot{\ell}(t)$ in (18) can be bounded as

$$|\dot{\ell}(\tau)| \leq K_1 d + v_{\max}$$

From (11) it follows that $\dot{x}_F(t)$, $\dot{y}_F(t)$ and $\dot{z}_F(t)$ are also bounded by

$$\begin{aligned}|\dot{x}_F(\tau)| &\le (K_1 d + v_{\max})(1 + (k_{1\max} + k_{2\max})d) + v_{\max}\\ |\dot{y}_F(\tau)| &\le (K_1 d + v_{\max})k_{1\max} d + v_{\max}\\ |\dot{z}_F(\tau)| &\le (K_1 d + v_{\max})k_{2\max} d + v_{\max}\end{aligned}$$

while $\dot{\theta}_e(\tau)$ and $\dot{\psi}_e(\tau)$ can be bounded as

$$|\dot{\theta}_e(\tau)| \le (K_1 d + v_{\max})k_{2\max} + |q(\tau)| + |r(\tau)|$$

$$|\dot{\psi}_e(\tau)| \le (K_1 d + v_{\max})(k_{1\max} + k_{2\max}\tan\nu_1) + \frac{|q(\tau)|}{\cos\nu_1} + \frac{|r(\tau)|}{\cos\nu_1}$$

where $k_{1\max}$ and $k_{2\max}$ are the maximum values of $|k_1(\ell)|$ and $|k_2(\ell)|$ along the path, respectively. Furthermore, $\dot{\phi}_e(\tau)$ can be bounded as an affine function of the roll rate $|p(\tau)|$, the pitch rate $|q(\tau)|$, and the yaw rate $|r(\tau)|$ as

$$|\dot{\phi}_e(\tau)| \le |p(\tau)| + \tan\nu_1|q(\tau)| + \tan\nu_1|r(\tau)| + k_{\phi_e}$$

for all $\tau \in [0, t]$ and some positive constant k_{ϕ_e}.

With the above results next we prove that if $x(\tau) \in \bar{\Omega}$ for all $\tau \in [0, t]$, then the outer-loop path-following commands $q_c(\tau)$ and $r_c(\tau)$ are bounded for all $\tau \in [0, t]$. To this effect, we expand the kinematic control law (19) as

$$\begin{aligned}q_c = &\cos\phi_e(u_{\theta_c} - \dot{\ell}k_2(\ell)\cos\psi_e) + \sin\phi_e\cos\theta_e(u_{\psi_c} + \dot{\ell}(k_1(\ell)\\ &- k_2(\ell)\tan\theta_e\sin\psi_e))\end{aligned} \tag{A11}$$

$$\begin{aligned}r_c = &-\sin\phi_e(u_{\theta_c} - \dot{\ell}k_2(\ell)\cos\psi_e) + \cos\phi_e\cos\theta_e(u_{\psi_c} + \dot{\ell}(k_1(\ell)\\ &- k_2(\ell)\tan\theta_e\sin\psi_e))\end{aligned} \tag{A12}$$

where we have used the fact that

$$T^{-1}(t, \theta_e) = \begin{bmatrix}\cos\phi_e & \sin\phi_e\cos\theta_e\\ -\sin\phi_e & \cos\phi_e\cos\theta_e\end{bmatrix}$$

It is now required to show that all the terms in (A11) and (A12) are bounded.

To show that $u_{\theta_c}(\tau)$, which was introduced in (20), is bounded, we first determine the time derivative of $\delta_\theta(\tau)$, which is given by

$$\dot{\delta}_\theta = \begin{cases}\frac{1}{\sqrt{1-(\frac{z_F}{z_F+d_1})^2}}\frac{d_1\dot{z}_F}{(z_F+d_1)^2} & z_F > 0\\ \frac{1}{\sqrt{1-(\frac{z_F}{-z_F+d_1})^2}}\frac{d_1\dot{z}_F}{(-z_F+d_1)^2} & z_F < 0\end{cases}$$

and because

$$-1 < \frac{-d}{d+d_1} \le \frac{z_F}{|z_F| + d_1} \le \frac{d}{d+d_1} < 1$$

and $\dot{z}_F(t)$ is bounded, one can conclude that the time derivative of $\delta_\theta(\tau)$ is bounded for all $\tau \in [0, t]$. Also, it is easy to check that

$$\lim_{z_F\to 0^+}\dot{\delta}_\theta = \lim_{z_F\to 0^-}\dot{\delta}_\theta = \frac{\dot{z}_F}{d_1}$$

Furthermore, the term $\frac{\sin\theta_e - \sin\delta_\theta}{\theta_e - \delta_\theta}$ is also bounded because

$$\lim_{\theta_e\to\delta_\theta}\frac{\sin\theta_e - \sin\delta_\theta}{\theta_e - \delta_\theta} = \lim_{\theta_e\to\delta_\theta}\cos\theta_e = \cos\delta_\theta$$

It follows from the results above that $u_{\theta_c}(\tau)$ is uniformly bounded for all $\tau \in [0, t]$. Similarly, it can be proven that $u_{\psi_c}(\tau)$ is also uniformly bounded for all $\tau \in [0, t]$, and therefore all the terms in (A11) and (A12) are bounded, which implies that the outer-loop path-following commands $q_c(\tau)$ and $r_c(\tau)$ are bounded. This result holds for all $\tau \in [0, t]$, and one can state that, as long as $x(\tau) \in \bar{\Omega}$, the following bounds hold:

$$\|q_{ct}\|_{\mathcal{L}_\infty} \le \gamma_{q_c}, \qquad \|r_{ct}\|_{\mathcal{L}_\infty} \le \gamma_{r_c} \tag{A13}$$

where γ_{q_c} and γ_{r_c} are some positive constants.

Next, we prove that the time derivatives of the outer-loop path-following commands $\dot{q}_c(\tau)$ and $\dot{r}_c(\tau)$ are also bounded. From (A11) and (A12), simple manipulations yield

$$\begin{aligned}\dot{q}_c = &-\dot{\phi}_e\sin\phi_e(u_{\theta_c} - \dot{\ell}k_2(\ell)\cos\psi_e)\\ &+ \cos\phi_e(\dot{u}_{\theta_c} - \ddot{\ell}k_2(\ell)\cos\psi_e - \dot{\ell}\dot{k}_2(\ell)\cos\psi_e\\ &+ \dot{\ell}k_2(\ell)\dot{\psi}_e\sin\psi_e) + (\dot{\phi}_e\cos\phi_e\cos\theta_e\\ &- \dot{\theta}_e\sin\phi_e\sin\theta_e)(u_{\psi_c} + \dot{\ell}(k_1(\ell) - k_2(\ell)\tan\theta_e\sin\psi_e))\\ &+ \sin\phi_e\cos\theta_e\Big(\dot{u}_{\psi_c} + \ddot{\ell}(k_1(\ell) - k_2(\ell)\tan\theta_e\sin\psi_e)\\ &+ \dot{\ell}\Big(\dot{k}_1(\ell) - \dot{k}_2(\ell)\tan\theta_e\sin\psi_e - \dot{\theta}_e k_2(\ell)\Big(\frac{1}{\cos\theta_e}\Big)^2\sin\psi_e\\ &- \dot{\psi}_e k_2(\ell)\tan\theta_e\cos\psi_e\Big)\Big)\end{aligned} \tag{A14}$$

and

$$\begin{aligned}\dot{r}_c = &-\dot{\phi}_e\cos\phi_e(u_{\theta_c} - \dot{\ell}k_2(\ell)\cos\psi_e)\\ &- \sin\phi_e(\dot{u}_{\theta_c} - \ddot{\ell}k_2(\ell)\cos\psi_e - \dot{\ell}\dot{k}_2(\ell)\cos\psi_e\\ &+ \dot{\ell}k_2(\ell)\dot{\psi}_e\sin\psi_e) - (\dot{\phi}_e\sin\phi_e\cos\theta_e\\ &+ \dot{\theta}_e\cos\phi_e\sin\theta_e)(u_{\psi_c} + \dot{\ell}(k_1(\ell) - k_2(\ell)\tan\theta_e\sin\psi_e))\\ &+ \cos\phi_e\cos\theta_e\Big(\dot{u}_{\psi_c} + \ddot{\ell}(k_1(\ell) - k_2(\ell)\tan\theta_e\sin\psi_e)\\ &+ \dot{\ell}\Big(\dot{k}_1(\ell) - \dot{k}_2(\ell)\tan\theta_e\sin\psi_e - \dot{\theta}_e k_2(\ell)\Big(\frac{1}{\cos\theta_e}\Big)^2\sin\psi_e\\ &- \dot{\psi}_e k_2(\ell)\tan\theta_e\cos\psi_e\Big)\Big)\end{aligned} \tag{A15}$$

First we notice that the time derivative of the rate of progression $\ddot{\ell}(t)$ can be bounded by an affine function of the pitch rate $q(t)$ and the yaw rate $r(t)$. To prove this we determine the time derivative of $\dot{\ell}(t)$, which is given by

$$\begin{aligned}\ddot{\ell} = &K_1\dot{x}_F + \dot{v}\cos\theta_e\cos\psi_e - v\dot{\theta}_e\sin\theta_e\cos\psi_e\\ &- v\dot{\psi}_e\cos\theta_e\sin\psi_e\end{aligned}$$

Again, since the AP is designed to stabilize the UAV, and the thrust and its rate of variation are limited, we can assume that the rate of variation of the UAV speed $\dot{v}(\tau)$ is bounded. Therefore, for all $\tau \in [0, t]$ the following bound holds:

$$|\ddot{\ell}(\tau)| \le k_{\ell 1}|q(\tau)| + k_{\ell 2}|r(\tau)| + k_{\ell 3}$$

where $k_{\ell 1}$, $k_{\ell 2}$, and $k_{\ell 3}$ are some positive constants.

Moreover, it can be proven that both $\dot{u}_{\theta_c}(\tau)$ and $\dot{u}_{\psi_c}(\tau)$ can also be bounded by affine functions of the pitch rate $|q(\tau)|$ and the yaw rate $|r(\tau)|$. In fact, from (20) it follows that

$$\begin{aligned}\dot{u}_{\theta_c} = &-K_2(\dot{\theta}_e - \dot{\delta}_\theta) + \frac{c_2}{c_1}\Big(\dot{z}_F v\frac{\sin\theta_e - \sin\delta_\theta}{\theta_e - \delta_\theta}\\ &+ z_F\dot{v}\frac{\sin\theta_e - \sin\delta_\theta}{\theta_e - \delta_\theta} + z_F v\frac{\mathrm{d}}{\mathrm{d}\tau}\Big(\frac{\sin\theta_e - \sin\delta_\theta}{\theta_e - \delta_\theta}\Big) + \ddot{\delta}_\theta\Big)\end{aligned}$$

where

$$\frac{\mathrm{d}}{\mathrm{d}\tau}\left(\frac{\sin\theta_e-\sin\delta_\theta}{\theta_e-\delta_\theta}\right)$$
$$=\frac{(\dot\theta_e\cos\theta_e-\dot\delta_\theta\cos\delta_\theta)(\theta_e-\delta_\theta)-(\sin\theta_e-\sin\delta_\theta)(\dot\theta_e-\dot\delta_\theta)}{(\theta_e-\delta_\theta)^2}$$

Then, since

$$\lim_{\theta_e\to\delta_\theta}\left(\frac{\mathrm{d}}{\mathrm{d}\tau}\left(\frac{\sin\theta_e-\sin\delta_\theta}{\theta_e-\delta_\theta}\right)\right)=-\frac{1}{2}\sin\delta_\theta(\dot\theta_e+\dot\delta_\theta)$$

this term can also be bounded by an affine function of $|q(\tau)|$ and $|r(\tau)|$. Finally, we can determine an expression for $\ddot\delta_\theta(\tau)$:

$$\ddot\delta_\theta=\frac{1}{\sqrt{1-(\frac{z_F}{|z_F|+d_1})^2}}\left(\frac{\frac{z_F}{|z_F|+d_1}}{1-(\frac{z_F}{|z_F|+d_1})^2}\frac{\mathrm{d}}{\mathrm{d}\tau}\left(\frac{z_F}{|z_F|+d_1}\right)+\frac{\mathrm{d}^2}{\mathrm{d}\tau^2}\left(\frac{z_F}{|z_F|+d_1}\right)\right)$$

where

$$\frac{\mathrm{d}}{\mathrm{d}\tau}\left(\frac{z_F}{|z_F|+d_1}\right)=\begin{cases}\frac{d_1\dot z_F}{(z_F+d_1)^2} & z_F>0\\ \frac{d_1\dot z_F}{(-z_F+d_1)^2} & z_F<0\end{cases}$$

and

$$\frac{\mathrm{d}^2}{\mathrm{d}\tau^2}\left(\frac{z_F}{|z_F|+d_1}\right)=\begin{cases}\frac{d_1\ddot z_F(z_F+d_1)-2d_1\dot z_F^2}{(z_F+d_1)^3} & z_F>0\\ \frac{d_1\ddot z_F(-z_F+d_1)+2d_1\dot z_F^2}{(-z_F+d_1)^3} & z_F<0\end{cases}$$

From (11) we can derive the following expression for the second-time derivative of z_F

$$\ddot z_F=-\ddot\ell k_2(\ell)x_F-\dot\ell\dot k_2(\ell)x_F-\dot\ell k_2(\ell)\dot x_F-\dot v\sin\theta_e-\dot\theta_e v\cos\theta_e$$

which turns out to be a function of $\ddot\ell(\tau)$ and $\dot\theta_e(\tau)$, and therefore it can also be bounded by an affine function of $|q(\tau)|$ and $|r(\tau)|$. This proves the bound on $\dot u_{\theta_c}(\tau)$. The bound on $\dot u_{\psi_c}(\tau)$ can be derived in a similar way. Hence, we have that $\dot q_c(\tau)$ can be bounded by an affine function of $|p(\tau)|$, $|q(\tau)|$, and $|r(\tau)|$. Similarly, we can prove that $\dot r_c(\tau)$ can also be bounded by an affine function of $|p(\tau)|$, $|q(\tau)|$, and $|r(\tau)|$. Therefore,

$$\begin{aligned}|\dot q_c(\tau)|&\le k_{q1}|p(\tau)|+k_{q2}|q(\tau)|+k_{q3}|r(\tau)|+k_{q4}\\ |\dot r_c(\tau)|&\le k_{r1}|p(\tau)|+k_{r2}|q(\tau)|+k_{r3}|r(\tau)|+k_{r4}\end{aligned}\tag{A16}$$

for all $\tau\in[0,t]$ and for some positive constants k_{q1}, k_{q2}, k_{q3}, k_{q4}, k_{r1}, k_{r2}, k_{r3}, and k_{r4}.

Using Lemmas 3 and 4 and the bounds in (A13), one can conclude that, for any $\tau\in[0,t]$, the $\mathcal{L}_1$ control signals $q_{\mathrm{ad}}(\tau)$ and $r_{\mathrm{ad}}(\tau)$ as well as the pitch rate $q(\tau)$ and the yaw rate $r(\tau)$, can be bounded as follows:

$$\begin{aligned}|q_{\mathrm{ad}}(\tau)|&\le k_{q_{\mathrm{ad}}1}\gamma_{q_c}+k_{q_{\mathrm{ad}}2},\qquad |r_{\mathrm{ad}}(\tau)|\le k_{r_{\mathrm{ad}}1}\gamma_{r_c}+k_{r_{\mathrm{ad}}2}\\ |q(\tau)|&\le \bar k_{q1}\gamma_{q_c}+\bar k_{q2},\qquad |r(\tau)|\le \bar k_{r1}\gamma_{r_c}+\bar k_{r2}\end{aligned}\tag{A17}$$

where $k_{q_{\mathrm{ad}}1}$, $k_{q_{\mathrm{ad}}2}$, $k_{r_{\mathrm{ad}}1}$, $k_{r_{\mathrm{ad}}2}$, $\bar k_{q1}$, $\bar k_{q2}$, $\bar k_{r1}$, and $\bar k_{r2}$ are positive constants that can be analytically computed using the derivations in [27].

Finally, since the $\mathcal{L}_1$ control signals $q_{\mathrm{ad}}(\tau)$ and $r_{\mathrm{ad}}(\tau)$ are bounded [see (A17)], the AP guarantees that both the bank angle $\phi(\tau)$ and the roll rate $p(\tau)$ are bounded (Assumption 3). Then, it follows from (A16) and (A17) that the derivatives of the commanded reference signals $q_c(t)$ and $r_c(t)$ are also bounded for all $\tau\in[0,t]$, and therefore, as long as $x(\tau)\in\bar\Omega$, the bounds

$$\|\dot q_{ct}\|_{\mathcal{L}_\infty}\le\gamma_{\dot q_c},\qquad \|\dot r_{ct}\|_{\mathcal{L}_\infty}\le\gamma_{\dot r_c}$$

apply for some positive constants $\gamma_{\dot q_c}$ and $\gamma_{\dot r_c}$.

Similar derivations can be used to show that, as long as $x(\tau)\in\bar\Omega$, the second derivatives of the commanded reference signals $q_c(t)$ and $r_c(t)$ are also bounded for all $\tau\in[0,t]$, i.e.,

$$\|\ddot q_{ct}\|_{\mathcal{L}_\infty}\le\gamma_{\ddot q_c},\qquad \|\ddot r_{ct}\|_{\mathcal{L}_\infty}\le\gamma_{\ddot r_c}$$

for some positive constants $\gamma_{\ddot q_c}$ and $\gamma_{\ddot r_c}$. □

Proof of Theorem 1: Using the same Lyapunov function candidate as in (22), it follows that

$$\dot V_{\mathrm{pf}}\le -x^\top\bar Q_{\mathrm{pf}}x+\frac{|\theta_e-\delta_\theta|}{c_2}|u_\theta-u_{\theta_c}|+\frac{|\psi_e-\delta_\psi|}{c_2}|u_\psi-u_{\psi_c}|\tag{A18}$$

where $\bar Q_{\mathrm{pf}}$ was defined in (53), and we have taken into consideration the errors between $u_\theta(t)$ and $u_{\theta_c}(t)$, and $u_\psi(t)$ and $u_{\psi_c}(t)$ (or equivalently between $q(t)$ and $q_c(t)$, and $r(t)$ and $r_c(t)$). Next we will show that, under the conditions of the Theorem, the terms $|\theta_e-\delta_\theta|$, $|u_\theta-u_{\theta_c}|$, $|\psi_e-\delta_\psi|$, and $|u_\psi-u_{\psi_c}|$ are bounded, and the original domain of attraction for the kinematic-error equations given in (21) becomes a positively invariant set for the path-following closed-loop dynamics.

Extending the proof in [31], we prove this Theorem by contradiction. Since $x(0)\in\Omega$, and $V_{\mathrm{pf}}(t)$ is continuous and differentiable, if (54) is not true, then there exists a time t' such that

$$V_{\mathrm{pf}}(\tau)<\frac{c}{2},\quad\forall\ \tau\in[0,t');\qquad V_{\mathrm{pf}}(t')=\frac{c}{2}\tag{A19}$$

which implies

$$\dot V_{\mathrm{pf}}(t')\ge 0\tag{A20}$$

It follows from Lemma 6 that the commanded reference signals $q_c(\tau)$ and $r_c(\tau)$ and their first and second derivatives are bounded for all $\tau\in[0,t']$, i.e.,

$$\begin{aligned}&\|q_{ct'}\|_{\mathcal{L}_\infty}\le\gamma_{q_c},\qquad \|\dot q_{ct'}\|_{\mathcal{L}_\infty}\le\gamma_{\dot q_c},\qquad \|\ddot q_{ct'}\|_{\mathcal{L}_\infty}\le\gamma_{\ddot q_c}\\ &\|r_{ct'}\|_{\mathcal{L}_\infty}\le\gamma_{r_c},\qquad \|\dot r_{ct'}\|_{\mathcal{L}_\infty}\le\gamma_{\dot r_c},\qquad \|\ddot r_{ct'}\|_{\mathcal{L}_\infty}\le\gamma_{\ddot r_c}\end{aligned}\tag{A21}$$

Therefore, from this result and the bounds on the initial conditions in (50) and (51), it follows that the bounds in (42) and (44) in Lemma 5 hold with $r_q(t)\equiv q_c(t)$, $r_r(t)\equiv r_c(t)$, and for any $\tau\in[0,t']$. As a consequence

$$\|(q-q_c)_{t'}\|_{\mathcal{L}_\infty}\le\gamma_\theta\qquad \|(r-r_c)_{t'}\|_{\mathcal{L}_\infty}\le\gamma_\psi\tag{A22}$$

Next, using (48), it follows that

$$\begin{aligned}u_\theta-u_{\theta_c}&=\cos\phi_e(q-q_c)-\sin\phi_e(r-r_c)\\ u_\psi-u_{\psi_c}&=\frac{\sin\phi_e}{\cos\theta_e}(q-q_c)+\frac{\cos\phi_e}{\cos\theta_e}(r-r_c)\end{aligned}$$

and hence, from the bounds in (A22), we have that

$$\|(u_\theta-u_{\theta_c})_{t'}\|_{\mathcal{L}_\infty}\le\gamma_{u_\theta}\qquad \|(u_\psi-u_{\psi_c})_{t'}\|_{\mathcal{L}_\infty}\le\gamma_{u_\psi}\tag{A23}$$

with γ_{u_θ} and γ_{u_ψ} defined in (49). Moreover, it follows from (A19) that for any $\tau\in[0,t']$ the following bounds apply:

$$|\theta_e(\tau)-\delta_\theta(\tau)|\le\sqrt{cc_2},\qquad |\psi_e(\tau)-\delta_\psi(\tau)|\le\sqrt{cc_2}\tag{A24}$$

Therefore, Eqs. (A18), (A23), and (A24) imply

$$\dot V_{\mathrm{pf}}(t')\le -x^\top(t')\bar Q_{\mathrm{pf}}x(t')+\sqrt{\frac{c}{c_2}}(\gamma_{u_\theta}+\gamma_{u_\psi})$$

Since

$$x^\top(\tau)\bar Q_{\mathrm{pf}}x(\tau)\ge\frac{\lambda_{\min}(\bar Q_{\mathrm{pf}})}{\lambda_{\max}(P_{\mathrm{pf}})}V_{\mathrm{pf}}(\tau),\quad\forall\ \tau\ge 0$$

where $\lambda_{\min}(\bar{Q}_{\mathrm{pf}})$ and $\lambda_{\max}(P_{\mathrm{pf}})$ are the minimum and the maximum eigenvalues of $\bar{Q}_{\mathrm{pf}}$ and P_{pf}, respectively, it follows from (A19) that, in particular, at time t' we have

$$x^{\top}(t')\bar{Q}_{\mathrm{pf}}x(t') \geq \frac{\lambda_{\min}(\bar{Q}_{\mathrm{pf}})}{\lambda_{\max}(P_{\mathrm{pf}})}\frac{c}{2}$$

Then, the design constraint in (52) leads to

$$\dot{V}_{\mathrm{pf}}(t') < 0$$

which contradicts (A20), and thus (54) holds for all $t \geq 0$. The upper bound in (54) implies that the bounds in (A2) hold for all $t \geq 0$, thus concluding the proof. □

Acknowledgments

Research is supported by the United States Special Operations Command under Tactical Network Training Grant, Office of Naval Research under Contracts N00014-08-WR-20287 and N00014-05-1-0828, U.S. Air Force Office of Scientific Resarch under Contract No. FA9550-08-1-0135, U.S. Army Research Office under Contract No. W911NF-06-1-0330, NASA under Contracts NNX08BA64 and NNX08BA65A, and European Commission under Contracts EU-FP6-IST-035223 (GREX), EU-FP7-ICT-231378 (Cognitive Cooperative Control for Autonomous Underwater Vehicles), and MRTN-CT-2006-036186 (FREESUBNET Training Network).

References

[1] Micaelli, A., and Samson, C., "Trajectory-Tracking for Unicycle-Type and Two-Steering-Wheels Mobile Robot," The French National Institute for Research in Computer Science and Control, Technical Report 2097, Sophia-Antipolis, France, 1993.

[2] Hindman, R., and Hauser, J., "Maneuver Modified Trajectory Tracking," in *International Symposium on Mathematical Theory of Networks and Systems*, St. Louis, MO, June 1996.

[3] Al-Hiddabi, S. A., and McClamroch, N. H., "Tracking and Maneuver Regulation Control for Nonlinear Non-Minimum Phase Systems," *IEEE Transactions on Control Systems Technology*, Vol. 10, No. 6, 2002, pp. 780–792. doi:10.1109/TCST.2002.804120

[4] Aguiar, A. P., and Hespanha, J., "Position Tracking of Underactuated Vehicles," in *American Control Conference*, 7839756, Vol. 3, University of California, Santa Barbara, CA, June 2003, pp. 1988–1993.

[5] Kaminer, I., Pascoal, A. M., Hallberg, E., and Silvestre, C., "Trajectory Tracking for Autonomous Vehicles: An Integrated Approach to Guidance and Control," *Journal of Guidance, Control and Dynamics*, Vol. 21, No. 1, Feb. 1998, pp. 29–38. doi:10.2514/2.4229

[6] Encarnação, P., "Nonlinear Path Following Control Systems for Autonomous Oceanic Vehicles," Ph.D., thesis, Instituto Superior Técnico, Lisbon,2000.

[7] Soetanto, D., Lapierre, L., and Pascoal, A. M., "Adaptive Non-Singular Path Following Control of Dynamics Wheeled Robots," *42nd IEEE Conference on Decision and Control*, Vol. 2, IEEE Publications, Piscataway, NJ, Dec. 2003.

[8] Cao, C., and Hovakimyan, N., "Design and Analysis of a Novel $\mathcal{L}_1$ Adaptive Control Architecture with Guaranteed Transient Performance," *IEEE Transactions on Automatic Control*, Vol. 53, No. 2, 2008, pp. 586–591. doi:10.1109/TAC.2007.914282

[9] Cao, C., and Hovakimyan, N., "Stability Margins of $\mathcal{L}_1$ Adaptive Control Architecture," *IEEE Transactions on Automatic Control*, Vol. 55, No. 2, 2010 (to be published).

[10] Cao, C., and Hovakimyan, N., "$\mathcal{L}_1$ Adaptive Controller for Systems with Unknown Time-Varying Parameters and Disturbances in the Presence of Non-Zero Initialization Error," *International Journal of Control*, Vol. 81, No. 7, 2008, pp. 1147–1161. doi:10.1080/00207170701670939

[11] Beard, R. W., Knoebel, N. B., Cao, C., Hovakimyan, N., and Matthews, J. S., "An $\mathcal{L}_1$ Adaptive Pitch Controller for Miniature Air Vehicles," AIAA Paper 2006-6777, August 2006.

[12] Patel, V. V., Cao, C., Hovakimyan, N., Wise, K., and Lavretsky, E., "$\mathcal{L}_1$ Adaptive Controller for Tailless Unstable Aircraft in the Presence of Unknown Actuator Failures,"*International Journal of Control*, Vol. 82, No. 4, 2009, 705–720. doi:10.1080/00207170802225955

[13] Wang, J., Patel, V. V., Cao, C., Hovakimyan, N., and Lavretsky, E., "Novel $\mathcal{L}_1$ Adaptive Control Methodology for Aerial Refueling with Guaranteed Transient Performance," *Journal of Guidance, Control, and Dynamics*, Vol. 31, No. 1, 2008, pp. 182–193. doi:10.2514/1.31199

[14] Dobrokhodov, V., Kitsios, I., Kaminer, I., Jones, K. D., Xargay, E., Hovakimyan, N., Cao, C., Lizarraga, M., and Gregory, I. M., "Flight Validation of a Metrics Driven $\mathcal{L}_1$ Adaptive Control," AIAA Paper 2008-6987, Aug. 2008.

[15] Dobrokhodov, V., Kitsios, I., Kaminer, I., Jones, K. D., Xargay, E., Hovakimyan, N., Cao, C., Lizarraga, M., and Gregory, I. M., "Flight Validation of a Metrics Driven $\mathcal{L}_1$ Adaptive Control," AIAA Paper 2008-6987, Aug. 2008.

[16] Wise, K., Lavretsky, E., and Hovakimyan, N., "Verifiable Adaptive Flight Control: UCAV and Aerial Refueling," AIAA Paper 2008-6658, Aug. 2008.

[17] Kitsios, I., Dobrokhodov, V., Kaminer, I., Jones, K. D., Xargay, E., Hovakimyan, N., Cao, C., Lizarraga, M. I., Gregory, I. M., Nguyen, N. T., and Krishnakumar, K. S., "Experimental Validation of a Metrics Driven $\mathcal{L}_1$ Adaptive Control in the Presence of General Unmodeled Dynamics," *AIAA Guidance, Navigation, and Control Conference*, 2009-6188. AIAA, Reston, VA, Aug. 2009.

[18] Gregory, I. M., Cao, C., Xargay, E., Hovakimyan, N., and Zou, X., "$\mathcal{L}_1$ Adaptive Control Design for NASA AirSTAR Flight Test Vehicle," in *AIAA Guidance, Navigation, and Control Conference*, 2009-5738, AIAA, Reston, VA, Aug. 2009.

[19] Leman, T., Xargay, E., Dullerud, G., and Hovakimyan, N., "$\mathcal{L}_1$ Adaptive Control Augmentation System for the X-48B Aircraft," *AIAA Guidance, Navigation, and Control Conference*, 2009-5619, AIAA, Reston, VA, Aug. 2009.

[20] Kaminer, I., Yakimenko, O., Dobrokhodov, V., Pascoal, A., Hovakimyan, N., Patel, V. V., Cao, C., and Young, A., "Coordinated Path Following for Time-Critical Missions of Multiple UAVs via $\mathcal{L}_1$ Adaptive Output Feedback Controllers," AIAA Paper number 2007-6409, Aug. 2007.

[21] Aguiar, A., Kaminer, I., Ghabcheloo, R., Pascoal, A. M., Xargay, E., Hovakimyan, N., Cao, C., and Dobrokhodov, V., "Time-Coordinated Path Following of Multiple UAVs over Time-Varying Networks using $\mathcal{L}_1$ Adaptation," AIAA Paper 2008-7131, Aug. 2008.

[22] Kaminer, I., Yakimenko, O., Pascoal, A., and Ghabcheloo, R., "Path Generation, Path Following and Coordinated Control for Time-Critical Missions of Multiple UAVs," in *American Control Conference*, No. 9-13, July 2006, pp. 4906–4913.

[23] Aguiar, A., Hespanha, J., and Kokotović, P., "Performance Limitations in Reference Tracking and Path Following for Nonlinear Systems," *Automatica*, Vol. 44, No. 3, 2008, pp. 598–610. doi:10.1016/j.automatica.2007.06.030

[24] Bishop, R. L., "There is More than One Way to Frame a Curve," *The American Mathematical Monthly*, Vol. 82, No. 3, 1975, pp. 246–251. doi:10.2307/2319846.

[25] Hanson, A. J., and Ma, H., "Parallel Transport Approach to Curve Framing," Indiana University Computer Science Department, Technical report TR425, 1995.

[26] Hassan K. Khalil, *Nonlinear Systems*, 3rd ed., Prentice–Hall, Upper Saddle River, NJ, 2002.

[27] Cao, C., and Hovakimyan, N., "$\mathcal{L}_1$ Adaptive Output Feedback Controller for Non-Strictly Positive Real Reference Systems," *AIAA Journal of Guidance, Control and Dynamics*, Vol. 32, No. 3, May–June 2009, pp. 717-726. doi:10.2514/1.40877

[28] Cao, C., and Hovakimyan, N., "Stability Margins of $\mathcal{L}_1$ Adaptive Controller: Part II," in *American Control Conference*, 2007.4282486, July 2007, pp. 3931–3936.

[29] Cloud Cap Technology, Inc., "Piccolo/Piccolo Plus Autopilots—A high integrated autopilots for small UAVs," http://cloudcaptech.com/.

[30] Dobrokhodov, V., Yakimenko, O., Jones, K. D., Kaminer, I., Bourakov, E., Kitsios, I., and Lizarraga, M., "New Generation of Rapid Flight Test Prototyping System for Small Unmanned Air Vehicles," AIAA Paper 2007-6567, Aug. 2007.

[31] Cao, C., Hovakimyan, N., Kaminer, I., Patel, V. V., and Dobrokhodov, V., "Stabilization of Cascaded Systems via $\mathcal{L}_1$ Adaptive Controller with Application to a UAV Path Following Problem and Flight Test Results," *American Control Conference*, 9887018, July 2007, pp. 1787–1792.